Comprehensive Study on Phased Antenna Array Based on Conventional and Shielded Butler Matrix for 2.4 GHz Applications

Muhannad Basem Haidar

Submitted to the
Institute of Graduate Studies and Research
in partial fulfillment of the requirements for the degree of

Master of Science
in
Electrical and Electronic Engineering

Eastern Mediterranean University
June 2017
Gazimağusa, North Cyprus

Approval of the Institute of Graduate Studies and Research

Prof. Dr. Mustafa Tümer
Director

I certify that this thesis satisfies the requirements as a thesis for the degree of Master of Science in Electrical and Electronic Engineering.

Prof. Dr. Hasan Demirel
Chair, Department of Electrical and Electronic Engineering

We certify that we have read this thesis and that in our opinion it is fully adequate in scope and quality as a thesis for the degree of Master of Science in Electrical and Electronic Engineering.

Asst. Prof. Dr. Rasime Uyguroğlu
Supervisor

Examining Committee

1. Prof. Dr. Hasan Amca _____

2. Prof. Dr. Şener Uysal _____

3. Asst. Prof. Dr. Rasime Uyguroğlu _____

ABSTRACT

In this work, a phased antenna array based on 4×4 Butler matrix is designed and simulated for 2.4 GHz applications using Roger RT 5880 as a substrate layer. CST SUIT STUDIO is used for this purpose.

Two different designs of phased antenna array are simulated; the first one was based on microstrip technology, which is used to design both the feeding network (Butler matrix) and antenna array. The objective is achieved by switching the main beam to ±14° and ±40°. The side lobe levels of -9.4dB and -8.2dB were obtained while the directivities were 12.4dBi and 11.5dBi when different input ports were applied. The physical size of the overall structure is about 621 cm^2.

An enhancement on antenna radiation pattern is obtained by using a strip line instead of microstrip line in the design of the Butler matrix. The antenna array is shielded at the top layer of the structure from the spurious radiation of Butler matrix radiation effect. The radiation pattern is obtained by making square slits on the top layer of the ground plane. The side lobe levels are reduced by 2.8dB and 0.3dB while the directivity is increased. The proposed design has deeper nulls and smaller physical size. The overall structure size is about 436.6 cm^2. The scanning angle directions does not change compared with the conventional design based on microstrip technology since the spacing between antenna elements is the same in both cases.

Keywords: Phased Antenna Array, Butler Matrix, Strip line, Shielded Antenna.

ÖZ

Bu çalışmada, Roger RT 5880 katmanı kullanılarak 2.4 GHz uygulamaları için 4×4 Butler matrisine dayalı fazlı anten dizisi tasarlanmış ve sonuçlar CST SUIT STUDIO benzetim yazılımı ile elde edilmiştir.

Fazlı anten dizi sistemi iki farklı tasarımda ele alınmıştır. Birinci tasarımda hem besleme ağı, hem de dizi anten, mikro şerit teknolojisi kullanılak elde edilmiştir. Amaçlandığı gibi ±14 ° ve ±40 ° yönlerinde, dört hüzme elde edilmiştir. Elde edilen ışıma deseninin yan lopları -9.4dB ve -8.2dB düzeylerindedir. Buna karşılık yönlendirmeler, farklı besleme noktaları kullanıldığında 12.4dBi ve 11.5dBi seviyelerindedir. Toplam yapının fiziksel boyutu yaklaşık 621 $cm^{2'}$dir.

Butler matrisinin tasarımında, mikro şerit hattı yerine şerit hattı kullanılması, Butler matrisinin besleme devresinden kaynaklanan sanal ışıma etkisinin izole edilmesine ve antenin ışıma yaratacak yapısının üst katmanda kalarak ışıma deseninde bir iyileşme elde edilmesine sebep olmuştur.

Işıma deseni, zemin düzleminin üst katmanında kare kesikler yaparak elde edilmiştir. Yan lob seviyeleri 2.8dB ve 0.3dB azaltılırken, yönlendirilmede artış elde edilmiştir. Önerilen tasarım daha derin boşluklara ve daha küçük fiziksel boyutlara sahiptir. Toplam yapı boyutu yaklaşık 436.6 cm^2. Anten elemanları arasındaki mesafe her iki durumda da eşit olarak alındığından tarama açıları değişim göstermemiştir.

Anahtar Kelimeler: Fazlı anten dizisi, Butler matrisi, şerit hattı, korunaklı antyen.

ACKNOWLEDGMENT

I would like to give my sincere gratitude and appreciation for the efforts of my supervisor Asst. Prof. Dr. Rasime Uyguroğlu and her continuous support throughout the period of my study.

I would also like to thank Prof. Dr. Şener Uysal and Prof. Dr. Hasan Amca. Without their instructions and valuable comments, this work would not be accomplished.

I express my deepest gratitude to my parents who got me through my educational life.

TABLE OF CONTENTS

LIST OF TABLES

LIST OF FIGURES

LIST OF SYMBOLS AND ABBREVATIONS

AAS	Adaptive Antenna System
AF	Array Factor
BM	Butler Matrix
BW	Bandwidth
DOA	Direction of Arrival
DSPU	Digital Signal Processing Unit
SBS	Switched Beam System
SIR	Signal to Interference Ratio
SLL	Side Lobe Level
SOI	Signal of Interest

Chapter 1

INTRODUCTION

1.1 General Overview

The definition “Smart Antenna” refers to the digital signal-processing unit in the antenna structure, which makes the system smart by means of signal processing, although from the first glance, one thinks the antenna is smart, but on the contrary, it is not. The unit inside of it gives the meaning. The algorithm is used to adjust and assign direction of the main beam by controlling the phase shift and the amplitude excited at each antenna input [1].

1.2 Smart Antenna System

Various studies focused on a smart antenna system as the number of users and the demand for wireless service increases, in addition, the need of wider coverage area and higher transmission quality. Moreover, rejecting the unwanted interference and focusing the radiation pattern toward the desired user [2]. All of these reasons push the researchers to employ the smart antenna system to overcome these problems.

Figure 1.1 illustrates the working principle of smart antenna system. Assume two antennas are located at two points in space, the digital signal processing unit (DSPU) measures the direction of arrival (DOA) of signal of interest (SOI) by computing the time delay from each antenna element. The DSPU adjusts the weights w1 and w2, which in turn adjusts the amplitude and excitation phase shift at the input of each

antenna element to produce a radiation pattern focused on the desired user and tuning out the undesired SOI [3].

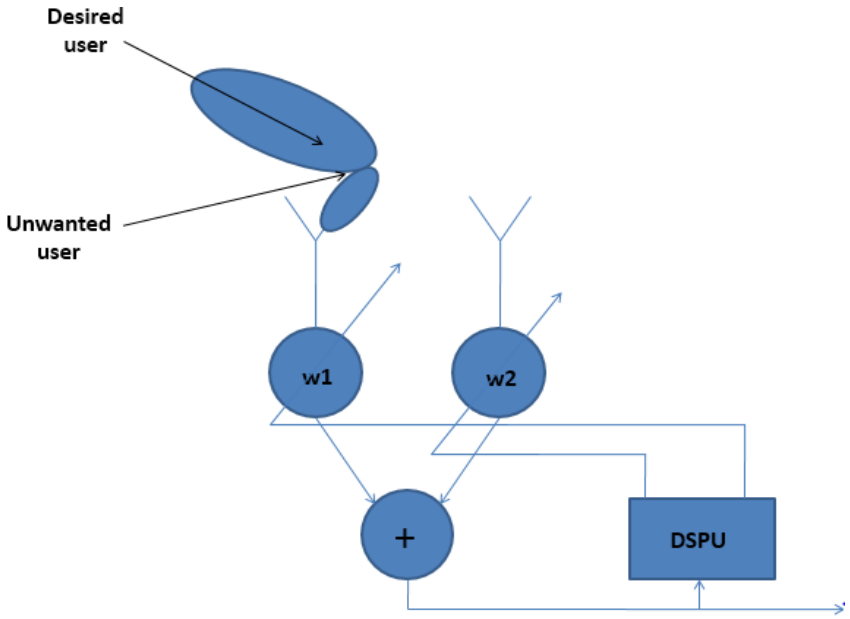

Figure 1.1: Smart antenna system.

Smart antenna system has two classifications, either switched beam system or adaptive antenna system.

1.2.1 Switched Beam System (SBS)

The SBS generates multiple overlapped patterns that cover the surrounded area; the system can choose one of these predefined patterns [2]. As the user moves throughout the cell, the SBS detects the signal strength and the base station determines the best beam that aligned in the SOI direction and switches to that beam to communicate with the user as shown in Figure1.2.a.

1.2.2 Adaptive Antenna System (AAS)

Adaptive antenna system (AAS) is smarter than (SBS) [4] [5]. It can continuously trace the user throughout the cell by steering the pattern towards the SOI while the nulls are steered in the direction of undesired SOI, which in turn, results in better signal to

interference ratio (SIR) [6], as shown in Figure 1.2.b. This procedure is done by the help of an adaptive array processor, which adopts the weights (complex) by an adaptive algorithm. That in turn changes the amplitude and phase shift to steer the main beam into the desired direction.

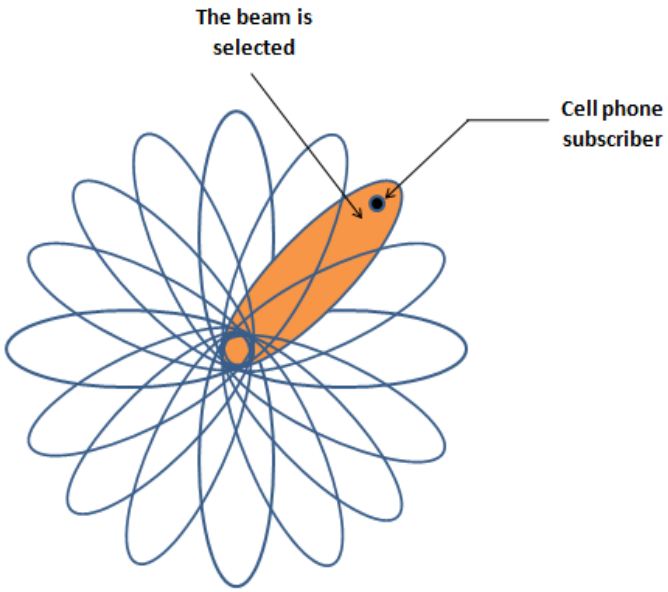

(a): Switched beam system

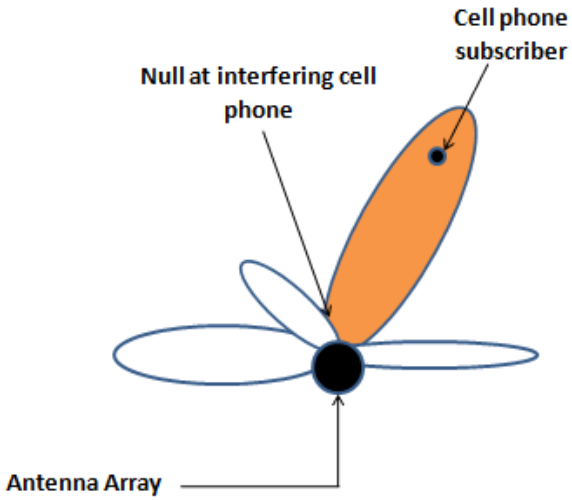

(b): Adaptive antenna system

Figure 1.2: (a): Switched beam system, (b): Adaptive antenna system.

1.3 Butler Matrix (BM)

1.3.1 Introduction

With the growth of wireless communication systems and techniques, the demand for higher capacity and good transmission quality is important. On the other hand, multiple users and multiple path signals propagation can degrade the quality of wireless communication systems due to the presence of co-channel interference and fading [7], which can be solved by the help of beam forming network with an antenna array by generating a beam of signals in the desired direction. Therefore, only the desired user can receive the signal and thus, the co-channel interference and fading is avoided.

Various kinds of beam forming networks can be connected to the antenna array such as BM (circuit based beam former), Rotman lens (lens based beam former), Blass and Nolen matrix. All of these solutions have capability of beam scanning by selecting one or more input/output ports [8]. However, the popularity of BM as a SBS feeding network takes many advantages, which are mentioned below.

1. Ease of fabrication process and low cost since it uses fewer and simple building blocks such as directional couplers, phase shifters and crossovers.
2. BM can generate continuous orthogonal beams without any mechanical motions, having narrower bandwidth (BW) and high directivity.

1.3.2 BM Structure

BM has 2^n input and 2^n output ports, where n=1, 2, 3... etc., so this kind of beam former called $N \times N$ BM where $N = 2^n$. It generates N orthogonal beams when it is connected to an antenna array, in addition to that, BM can cover from -180° up to 180° according to the type of elements used in the array and the spacing between antenna elements [9].

BM also consists of $\frac{N}{2}\log_2(N)$ directional couplers and $\frac{N}{2}(\log_2(N)-1)$ phase shifters to select the desired pattern [10]. Figure 1.3 shows a block diagram of 4×4 BM which contains 4 hybrid (3-dB) couplers, 2 crossovers (0-dB) and 2 phase shifters.

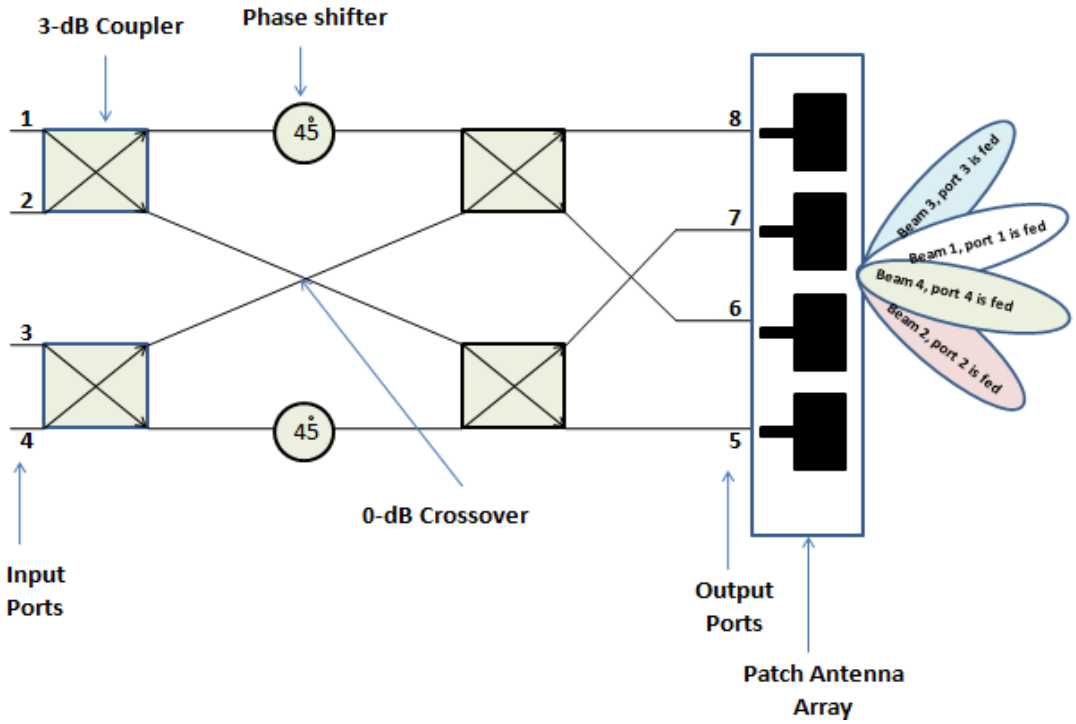

Figure 1.3: BM block diagram.

From Figure 1.3, it is easy to see that N orthogonal beams will be generated when the signal is excited from each input port individually. The phase difference φ at output ports of BM can control the direction of the main beam, as an example, if port 1 was the feeding port then the phase difference is φ between output ports and hence the antenna array can generate beam 1 as shown in Figure 4 and so on. In general, the phase difference between input and output ports can be summarized in the following Table:

Table 1.1: Ideal phase shift between different ports of the BM.

Output Ports / Input Ports	Port 5	Port 6	Port 7	Port 8	φ average
Port 1	0°	45°	90°	135°	45°
Port 2	0°	-135°	90°	-45°	-135°
Port 3	0°	135°	-90°	45°	135°
Port 4	0°	-45°	-90°	-135°	-45°

From Table 1.1, it is obvious that if port 1 is the feeding port, that means the phase difference between output ports relative to port 1 equal to 45°. Now, to determine the beam direction when $\varphi = 45$ degree, the phased antenna array equations in chapter two can do this. So, from the previous illustrations, two factors can effect the steerable beam, the phase shift between adjacent output ports in BM and the distance between adjacent elements.

In 1961, J. Butler and R. Lowe firstly introduced BM [11]. Many researchers employed it to solve the problems of interference and precise detection of the desired user, and hence, it has been studied and improved by many antenna researchers to be adopted to the new technologies used in communication systems. BM as a beamforming network can be considered as a SBS [6] , which has a capability to cover 360° coverage area when it is combined to an antenna array [10]. The physical structure size of SBS based on BM is another important factor, so, the phase shifter can be designed based on T-shaped array defected microstrip structure (ADMS) to reduce the width of the overall structure with an acceptable coupling factors at the output of BM [12].

For large BW, the design of N×N wideband BM should be achieved. So, in order to cover the IEEE 802.11b/g/n band, a 4×4 wide band, BM based on wide band 90̊ hybrid couplers and crossovers is considered to cover the band from 2.1 GHZ 2.75 GHz [13]. On the other hand, to decrease the power distribution and phase error at the output of BM, back to back bilayer microstrip method is applied without using crossover [14]. The proposed structure is suitable for 4.3 GHz applications by using 8×8 BM with an acceptable reurn losses and isolations between feeding ports. Anew method to design and implement the crossover is by cutting the ground plane and take the connection from there. Based on this method a size reduction of BM is achieved [15].

The overall goal of SBS based on beamforming network is in increase the gain towards the desired user while the side lobe levels should be reduced. This can be achieved by adding 180̊ Power divider at the output of BM and hence the BM becomes N×2N instead of N×N which in turns doubled the number of an antenna elements at the output of BM [16]. On the other hand, a Wilkinson power divider is used to obtain tapered output amplitude distribution and to achieve SLL reduction [17]. The interference problem is reduced by cascading two 3-dB wide band hybrid coupler to obtain wide band crossover in order to form 4×4 BM for multibeam phased antenna array for 1.9 GHz with good performance in terms of phase and power distribution error [18].

1.4 Thesis Objective

In this work, a shielding method based on strip line technology with proximity coupling feed technique is applied to shield the radiation pattern of microstrip antenna array from the spurious radiation of microstrip line BM network. Which in turn can enhance the beam pattern shape with lower levels of side lobes.

Chapter 2

MICROWAVE COMPONENTS

2.1 Introduction

As mentioned in Chapter 1, the BM consists of microwave components such as branch line couplers, phase shifters and crossovers which are combined to antenna array. In this chapter, a full description will be introduced to understand the behavior and properties of these components.

2.2 Microwave Components

2.2.1 Directional Couplers

Directional couplers can be considered as passive four ports equal/unequal power divider that the input signal is divided equally/unequally into two or more output signals. The coupler usually has lossless ports; it can be designed as an equal power divider. As a special case of directional coupler is the hybrid quadrature coupler which have an equal power with 90° phase shift at the output ports [11].

The directional coupler has four matched ports. For the ideal directional coupler (reciprocal and lossless), the scattering parameters are shown in equation (2.1):

$$[S] = \begin{bmatrix} 0 & S_{12} & S_{13} & S_{14} \\ S_{12} & 0 & S_{23} & S_{24} \\ S_{13} & S_{23} & 0 & S_{43} \\ S_{14} & S_{24} & S_{43} & 0 \end{bmatrix} \quad (2.1)$$

Where $S_{ij} = S_{ji}$ for $i, j = 1,2,3$ and 4. Since the network is lossless, 10 equations mentioned in [19] and [20] must be satisfied and hence, there are two choices to describe the directional couplers:

Symmetric coupler

This kind of directional coupler has the following scattering matrix:

$$[S] = \begin{bmatrix} 0 & \alpha & j\beta & 0 \\ \alpha & 0 & 0 & j\beta \\ j\beta & 0 & 0 & \alpha \\ 0 & j\beta & \alpha & 0 \end{bmatrix} \tag{2.2}$$

An anti-symmetric coupler

This kind of directional coupler has the following scattering matrix:

$$[S] = \begin{bmatrix} 0 & \alpha & \beta & 0 \\ \alpha & 0 & 0 & -\beta \\ \beta & 0 & 0 & \alpha \\ 0 & -\beta & 0 & \alpha \end{bmatrix} \tag{2.3}$$

Where β is the coupling factor and the constant $\alpha^2 = 1 - \beta^2$.

Assume that port 1 is the input port, ports 2 and 3 are the through and coupled ports while the fourth port is an isolated port, to obtain the coupling, directivity, isolation and insertion loss, the following quantities have to be used:

$$Coupling = C = 10\log\frac{P1}{P3} = -20\log\beta \; dB \tag{2.4}$$

$$Directivity = D = 10\log\frac{P3}{P4} = 20\log\frac{\beta}{|S14|} \; dB \tag{2.5}$$

$$Isolation = I = 10\log\frac{P1}{P4} = -20\log|S14| \; dB \tag{2.6}$$

$$Insertion\ Loss = L = 10\log\frac{P1}{P2} = -20\log|S12| \; dB \tag{2.7}$$

2.2.1.1 Conventional Hybrid Quadrature 90° Coupler

This type of coupler can be considered as a special case of directional coupler which allows the signal to be divided equally between the coupled and the direct port, while

remaining port is isolated (i.e, the coupling factor is 3-dB that implies $\alpha = \beta = \frac{1}{\sqrt{2}}$) with 90° phase shift at the output ports as shown in Figure 2.1. The scattering parameters in this case can be shown in (2.8), while the design of this kind of couplers can be obtained from its even and odd mode analysis as shown in Figure 2.2.

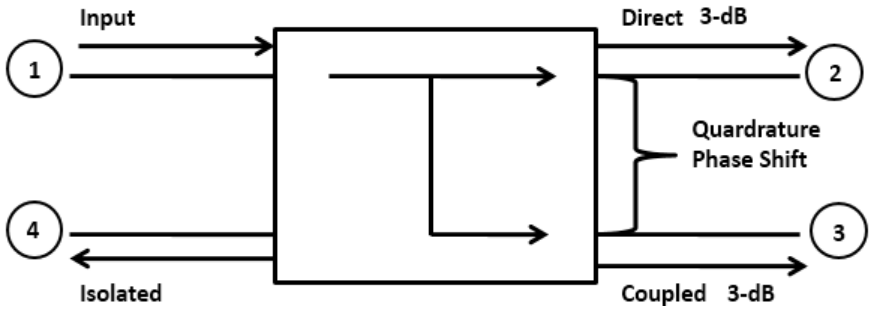

Figure 2.1: 3-dB quadrature hybrid coupler block diagram.

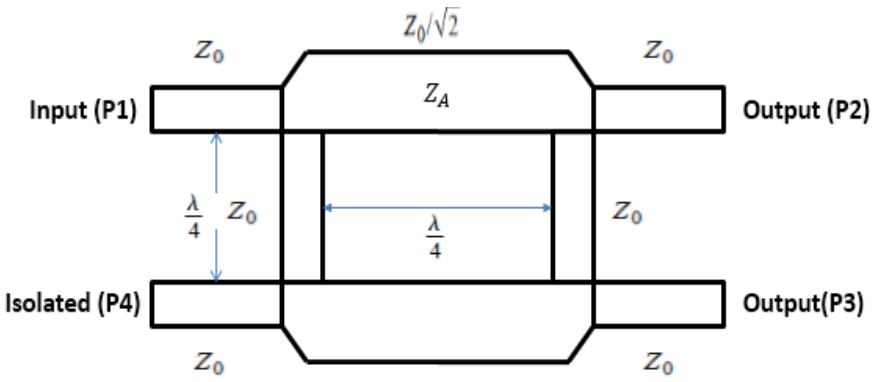

Figure 2.2: Geometry of 3-dB quadrature hybrid coupler.

$$[S] = \frac{1}{\sqrt{2}} \begin{bmatrix} 0 & 1 & j & 0 \\ 1 & 0 & 0 & j \\ j & 0 & 0 & 1 \\ 0 & j & 1 & 0 \end{bmatrix} \tag{2.8}$$

2.2.2 Crossovers

Crossover is a four-port network type, which is classified to be one of the transmission line circuits. The crossover is obtained by cascading two hybrids such that cascading two narrowband hybrids give a narrowband crossover while cascading two broadband

hybrids give broadband crossover. Crossovers must assure isolation between signals at the crossing lines as shown in Figure 2.3 [18].

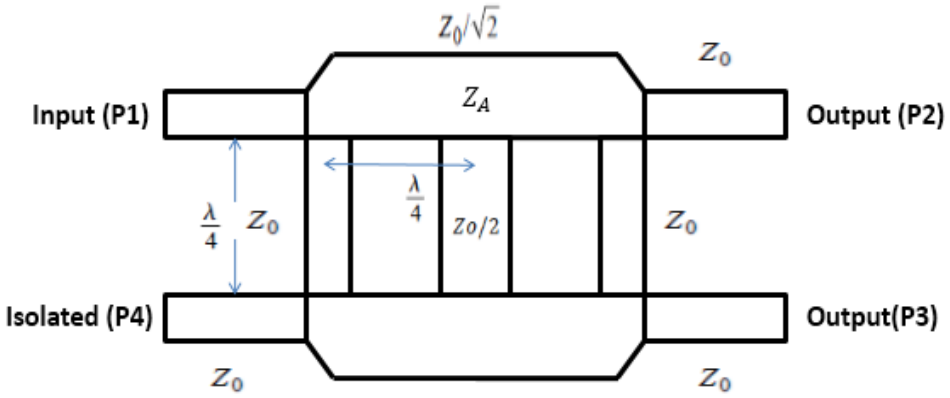

Figure 2.3: Geometry of conventional crossover.

The scattering parameters for the crossover are shown in the following scattering matrix [6].

$$[s] = \begin{bmatrix} 0 & 0 & j & 0 \\ 0 & 0 & 0 & j \\ j & 0 & 0 & 0 \\ 0 & j & 0 & 0 \end{bmatrix} \tag{2.9}$$

From the above scattering matrix, the following results can be concluded:

1. If port 1 is the input port, then S_{11}, S_{12} and S_{14} are equal to $-\infty$ while S_{13} is equal to 0-dB
2. If port 2 is the input port, then S_{22}, $S_{21}$and S_{23} are equal to $-\infty$ while S_{24} is equal to 0-dB
3. If port 3 is the input port, thenS_{33}, S_{32} and S_{34} are equal to $-\infty$ while SS_{31} is equal to 0-dB.
4. If port 4 is the input port, thenS_{44}, S_{41} and S_{43} are equal to $-\infty$ while S_{42} is equal to 0-dB.

2.2.3 Phase Shifters

The phase shifters are designed based on, either microstrip or strip lines, aiming to obtain a delay in the phase shift between two lines. This may be achieved by means of adding extra length as shown in Figure 2.4. As a result, line 2 is longer than line 1 by ΔL.

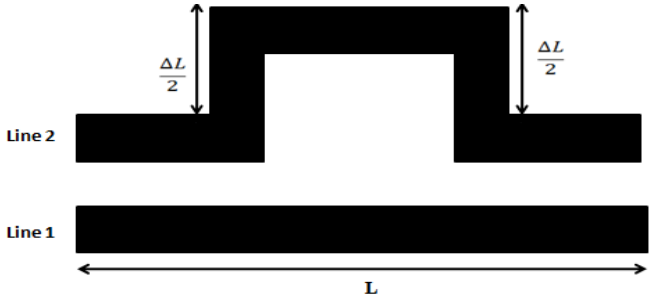

Figure 2.4: Phase shifter.

The phase θ_1 between input and output port of line 1 is given by

$$\theta_1 = \beta l_1 \tag{2.10}$$

Where $\beta = \frac{2\pi}{\lambda_g}$ and β is the phase constant.

The phase θ_2 between input and output port of line 2 is given by

$$\theta_2 = \beta l_2 \tag{2.11}$$

Where l_2=$l_1 + \Delta l$

The phase difference at the output ports between line 2 and 1 is given by

$$\theta_2 - \theta_1 = \Delta\theta = \frac{2\pi}{\lambda_g}\Delta l \tag{2.12}$$

Where λ_g is the guided wave length [7].

2.3 Microstrip Antennas

Microstrip antennas, also known as patch antennas were introduced and became extremely popular in 1970's [2]. It consists of metallic patch placed on dielectric substrate placed on a thin ground plane as shown in Figure 2.5. This kind of antenna can take various configurations such as rectangular, square, circular and circular ring

shape. Microstrip antenna received considerable attention due to its advantages which mentioned below [21]:

Simple and cheap for manufacturing, fabrication and installation,

1. Low profile,
2. Versatile in terms of resonant frequency, input impedance and radiation pattern,
3. Compatible with monolithic microwave integrated circuit (MMIC) designs.

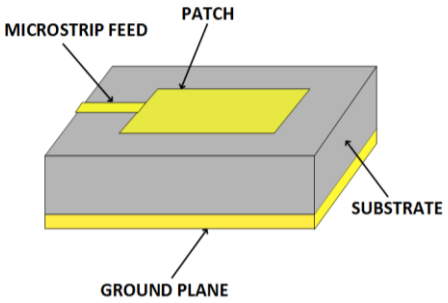

Figure 2.5: Microstrip antenna structure.

The metallic patch and ground plane have usually the same characteristics. The thickness of both of them is very thin ($t \ll \lambda_0$) where λ_0 is the wavelength in the free space. On the other hand, the dielectric layer thickness is in the range of ($0.003\lambda_0 \leq h \leq 0.05\lambda_0$). Moreover, it has a dielectric constant in the range of ($2.2 \leq \varepsilon_r \leq 12$). The ones that have dielectric constant in the lower end of this range with thick substrate provide better antenna efficiency and larger BW. However, the option of thin substrate selection with higher dielectric constant is suitable for microwave circuits to minimize undesired radiation and coupling which in turn lead to small circuit size.

2.3.1 Microstrip Feeding Types

Various techniques can be used to feed the microstrip antenna. The mainly four techniques used are:

1. Microstrip feeding lines.
2. Coaxial probe lines.

3. Aperture coupling technique.
4. Proximity coupling technique.

Each technique of the above-mentioned techniques can be used according to the desired antenna performance. In the following subsections, each technique will be summarized and introduced based on antenna performance and desired characteristics.

2.3.1.1 Microstrip Feeding Lines

The microstrip line is connected directly to the microstrip antenna as shown previously in Figure 2.5. The microstrip line is a conducting strip that has smaller width compared with microstrip antenna width. The popularity of this technique is due to easy of fabrication and simplicity of matching with antenna itself when the impedances are not equal. The matching can be achieved by using quarter wavelength transformer technique or controlling inset position [22].

2.3.1.2 Coaxial Probe Lines

The coaxial probe line consists of two conductors, inner and outer conductor. The outer conductor is connected to the ground plane surface while the inner conductor is extended until it connects the patch surface in the upper side as shown in Figure 2.6. The feeding to the antenna can be achieved from the lower layer of ground plain, and the matching can be maintained by adjusting the feeding position. This method is easy to fabricate and has low spurious radiation [22].

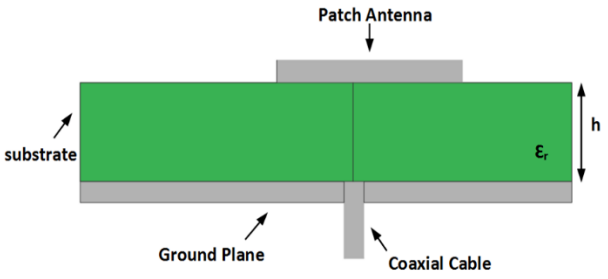

Figure 2.6: Coaxial probe feeding line.

2.3.1.3 Aperture Coupling

This technique can be considered as the most difficult technique among the four techniques of feeding. Two substrates are used separated by a ground plane, while the microstrip line is located on the bottom side of lower substrate whose radiation pattern is coupled through a slit on the ground plane as shown in Figure 2.7. The option of selecting substrate types will not be random. The selection must satisfy wide range of BW. This can be achieved by choosing a very thin with high dielectric constant for bottom substrate while another substrate could be thick with lower dielectric constant [22] [23].

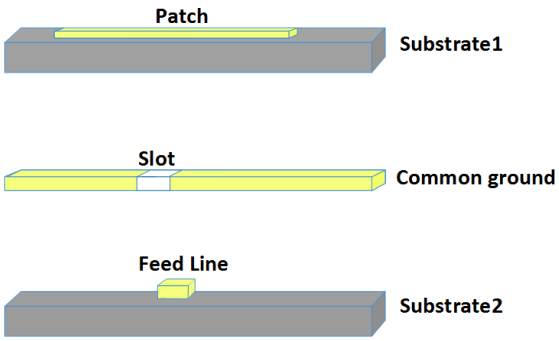

Figure 2.7: Aperture coupling.

2.3.1.4 Proximity Coupling

In this technique, two substrates will be used, both of the substrates will be one on top of the other, where the ground plane will be at the lower layer and the patch on the other side of the substrate, where the feeding line is sandwiched between the two substrates, as shown in Figure 2.8. By regulating the terminated stub, 13% fractional BW can be accomplished. The substrate selection have to be taken into consideration to improve the antenna bandwidth [24].

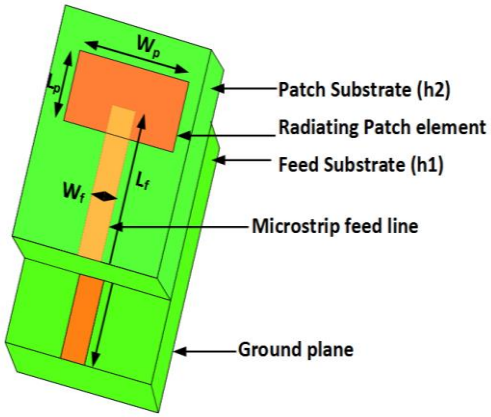

Figure 2.8: Proximity coupling.

2.3.2 Transmission Line Model

Though it has low accuracy, the transmission line model can be considered as the suitable approach for microstrip line analysis compared to full wave and cavity model. Antenna has been represented by three parameters; antenna width$W$, height of the substrate h and the antenna length L. Figure 2.9 represents transmission line model concept. The microstrip line positioned on top of the dielectric substrate, where the air will be the other substrate. Figure 2.10 shows the behavior of electrical field lines for the aforementioned case, it's clear that the majority of the electric fields are distributed in the dielectric region while the rest of it will lost in the air [21].

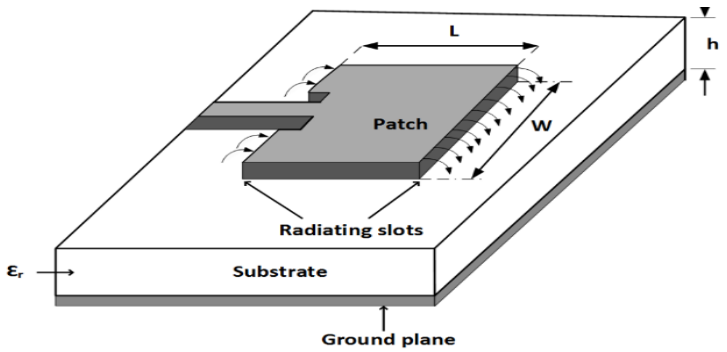

Figure 2.9: Transmission line model.

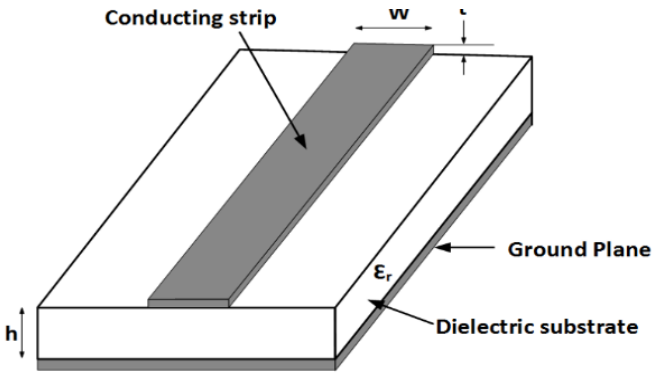

(a): Microstrip line

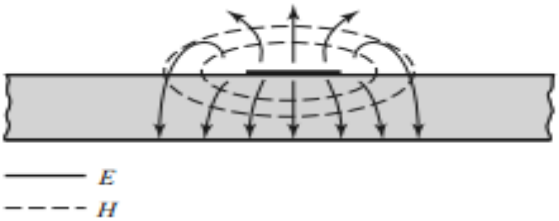

(b): Electric field distribution

Figure 2.10: (a) Microstrip line structure, (b) Cross section shows the electric and magnetic field distribution of (a).

The fringing field in the microstrip line has identical electrical characteristics as shown in Figure 2.10 and hence, the effective dielectric constant ε_{eff} must be taken into account which is in the range of $1 < \varepsilon_{eff} < \varepsilon_r$ [2]. Microstrip patch antennas radiate due to the fringing fields created between the patch and the ground plane. It resonates according to the dimensions of the radiating patch.

2.4 Phased Antenna Array

Many kinds of antennas like wire antennas, aperture antennas, resonant antennas and travelling wave antennas [21], can be considered as single element antennas. Most of these kinds suffered from lack of flexibility and gain. Moreover, single element antennas could not be considered as a good solution for tracking applications since the antenna radiation pattern for the above types cannot be controlled to be in the desired

direction. So far, the development of antenna array had been proposed to overcome the above problems.

Antenna array consists of more than one element arranged in a specific manner to achieve the desired antenna characteristics and performance. The total radiated field of the array is calculated by vector addition of the fields radiated by individual element. Therefore, to provide a very directive pattern, the radiated field of each single element must interfere constructively (in phase) in the desired direction and to interfere destructively (out of phase) in the other directions to minimize the side lobe level (SLL). Other approaches will be discussed in the coming sections that is used to shape the overall pattern such as [2]:

1. Controlling the amplitude and excitation phase shift between individual elements.
2. The distance between adjacent elements.

Antenna array can take many configurations. The most popular configurations are linear, planar and circular. In this work, a linear antenna array arrangement is used to provide a directive pattern in some direction fed by beam forming network.

Figure 2.11 shows a typical antenna of N-elements arranged in linear way. The far field radiation from an isotropic source can be expressed as [21]:

$$E_{ie} = \frac{e^{-j\beta r}}{4\pi r} \tag{2.13}$$

Where β is the Phase constant and r is the distance between isotropic source and the observation point. The total radiation field of an isotropic linear array is:

$$E_{ia} = E_{ie} \times \sum_{n=1}^{N} A_n \, e^{j\varphi_n} \tag{2.14}$$

Where A_n is the amplitude of element n and φ_n is the relative phase (to a common reference) of element n. The second term of (2.14) is called the isotropic array factor (AF).

$$AF = \sum_{n=1}^{N} A_n \, e^{j\varphi_n} \tag{2.15}$$

As shown in Figure 2.11, the spacing between antenna array elements is d and assuming that they have the same amplitude but each succeeding element has a progressive phase shift φo lead the current excitation relative to the proceeding one [21], in this case the uniform AF can be expressed as:

$$AF = \sum_{n=1}^{N} e^{j(n-1)\varphi} = e^{j[(N-1)/2]\varphi} \left[\frac{sin\,(N\varphi/2)}{sin(\varphi/2)}\right] \tag{2.16}$$

Where $\varphi = \beta d \sin\theta + \varphi_o$, $\beta = \frac{2\pi}{\lambda}$ and λ is the free space wave length. The maximum array factor is equal to N and so, the normalized Array factor is equal to:

$$AF_n = \frac{1}{N}\left[\frac{sin\,(N\varphi/2)}{sin(\varphi/2)}\right] \tag{2.17}$$

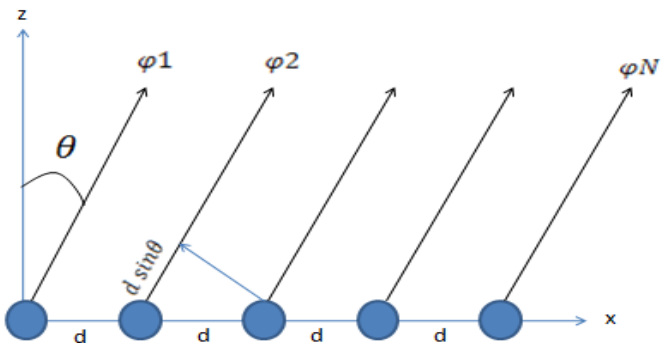

Figure 2.11: Typical antenna of N-elements arranged in linear way.

The maximum radiation occurs when φ equal to zero, and thus the main lobe direction θ will be directed according to 2.16 to:

$$\theta = -sin^{-1}\left(\frac{\lambda\varphi_o}{2\pi d}\right) \tag{2.18}$$

Chapter 3

DESIGN AND SIMULATION RESULTS

3.1 Introduction

In this chapter, a BM will be designed and simulated for 2.4 GHz applications. First, a conventional 4×4 BM using microstrip line technology is presented in details. A motivated method is applied on BM having the same properties of the conventional one using shielded antenna array and strip line technology in order to form the feeding network. Hence, the SLL is reduced and the directivity of phased antenna array is increased. The following subsections introduce the conventional and modified designs to compare their performances.

3.2 Analysis and Design of the Components of 4×4 Conventional BM Based on Microstrip Line Technology

The conventional BM consists of three main parts which are:

1. Branch line couplers (3 dB hybrid coupler).
2. Crossovers.
3. Phase shifters

3.2.1 Branch Line Coupler Design and Simulation Results

The branch line coupler or 3-dB hybrid coupler consists of a main line having an impedance of 50Ω which is coupled with a secondary line by two quarter wave length sections having an impedance of 35.35Ω spaced one quarter wave length apart as discussed in Chapter 2.

In order to find the widths and lengths of coupler main lines, microstrip line equations will be used.

$$Zo = \begin{cases} \frac{60}{\sqrt{\varepsilon_{eff}}} \ln\left(\frac{8h}{W} + \frac{W}{4h}\right) & \text{for } \frac{W}{h} \leq 1 \\ \frac{120\pi}{\sqrt{\varepsilon_{eff}}\left[\frac{W}{h} + 1.393 + 0.667 + \ln\left(\frac{W}{h} + 1.444\right)\right]} & \text{for } \frac{W}{h} \geq 1 \end{cases} \quad (3.1)$$

also,

$$\frac{W}{h} = \begin{cases} \frac{8e^{A}}{e^{2A} - 2} & \text{for } \frac{W}{h} \leq 2 \\ \frac{2}{\pi}(B - 1 - \ln(2B - 1)) + \frac{2}{\pi}\frac{\varepsilon_r - 1}{2\varepsilon_r}\left\{\ln(B - 1) + 0.39 - \frac{0.61}{\varepsilon_r}\right\} & \text{for } \frac{W}{h} \geq 2 \end{cases} \quad (3.2)$$

where;

$$A = \frac{Zo}{60}\sqrt{\frac{\varepsilon_r + 1}{2}} + \frac{\varepsilon_r - 1}{\varepsilon_r + 1}\left(0.23 + \frac{0.11}{\varepsilon_r}\right) \quad (3.3)$$

$$B = \frac{377\pi}{2Zo\sqrt{\varepsilon_r}} \quad (3.4)$$

$$\varepsilon_{eff} = \frac{\varepsilon_r + 1}{2} + \frac{\varepsilon_r - 1}{2\sqrt{1 + 12\frac{h}{W}}} \quad (3.5)$$

where;

Zo: Characteristic impedance

h: Substrate thickness

ε_r: Substrate relative permittivity

ε_{eff}: Substrate effective relative permittivity

Based on the above equations, the coupler parameters can be designed easily. Table 3.1 shows the summary of the coupler parameters using Roger RT 5880 substrate for 2.4 GHz applications.

Table 3.1: Coupler parameters.

Parameter	Value
f_r	2.4 GHz
ε_r	2.2
h	1.6 mm
$W_{(50\Omega)}$	4.9 mm
$W_{(35.35\Omega)}$	7.62 mm
$\varepsilon_{eff(50\Omega)}$	1.87
$\varepsilon_{eff(35.35\Omega)}$	1.92
$\lambda_{g(50\Omega)}/_4$	17.95 mm
$\lambda_{g(35.35\Omega)}/_4$	21 mm

According to Table 3.1, the coupler can be designed and simulated using CST SUITE STUDIO. Figure 3.1 shows a schematic diagram of branch line with its input and output ports.

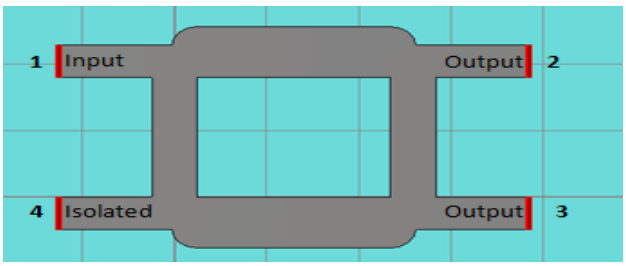

Figure 3.1: Designed branch line coupler.

The performance of 3-dB coupler was checked by testing the isolation, and the phase difference among the output ports, in addition to the return and coupling losses of the coupler. Figures 3.2 and 3.3 show the scattering parameters for branch line coupler and the phase difference between output ports when port 1 was fed as an input port.

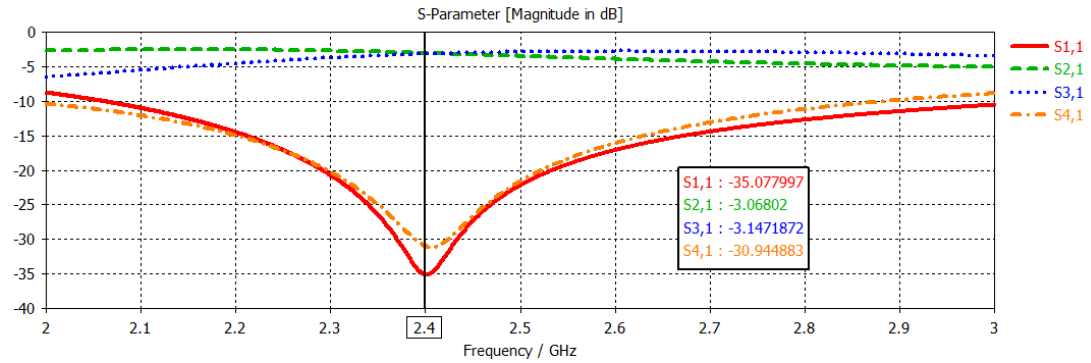

Figure 3.2: Coupler return loss, insertion loss and isolation loss.

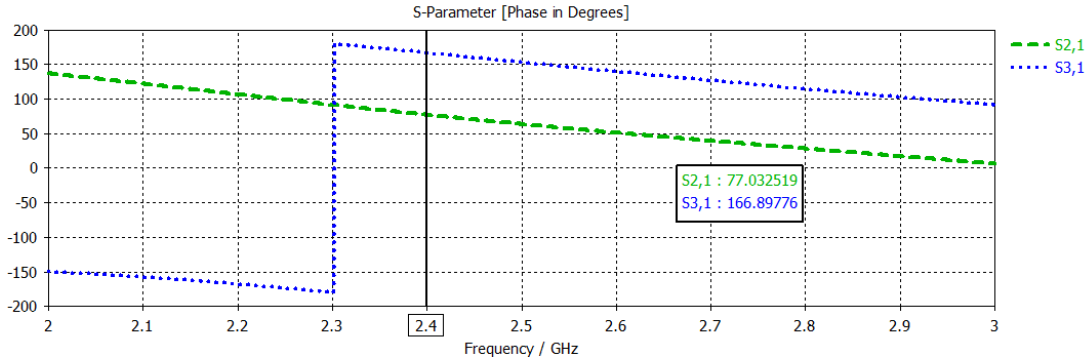

Figure 3.3: Phase difference between output ports.

Figure 3.2 shows the coupling, return and the isolation losses for the 3-dB coupler. The return loss S_{11} and isolation loss S_{41} are about -35dB and -31dB respectively. Hence, it is concluded that the designed coupler is roughly matched; on the other hand, the adjacent port 4 was isolated based on the value of S_{41}which is below -10dB. The coupling S_{21} and S_{31} are about -3dB which means that the power is divided equally between output ports. In terms of the phase shift, the phase difference between the output ports was 90̊ as shown in Figure 3.3. This means that the output signal at output ports are almost in phase quadrature when port 1 was the excitation port.

3.2.2 Crossover Design and Simulation Results

As mentioned in Chapter 2, cascading two branch line couplers results in a crossover. The objective of this design is to eliminate the mixture of signals, so isolation between

signals at the crossing lines is achieved. Table 3.2 summarizes crossover parameter dimensions using Roger RT 5880 for 2.4 GHz applications.

Table 3.2: Crossover parameters.

Parameter	Value
f_r	2.4 GHz
ε_r	2.2
h	1.6 mm
$W_{(50\Omega)}$	4.9 mm
$W_{(35.35\Omega)}$	7.1
$W_{(25\Omega)}$	10 mm
$\varepsilon_{eff(50\Omega)}$	1.87
$\varepsilon_{eff(35.35\Omega)}$	1.91
$\varepsilon_{eff(25\Omega)}$	1.95
$\lambda_{g(50\Omega)}/_4$	17.952 mm
$\lambda_{g(35.35\Omega)}/_4$	21 mm

According to the parameter dimensions mentioned in Table 3.2, it is simple to construct the crossover design as shown in Figure 3.4.

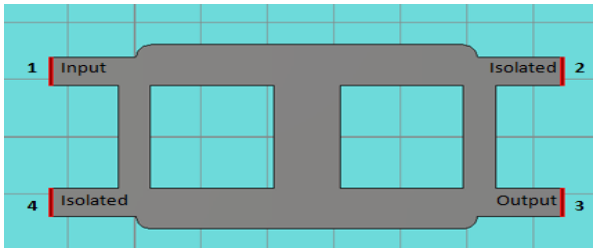

Figure 3.4: Crossover design using microstrip line.

The performance of the designed crossover was tested by checking its scattering parameters. In perfect crossover, all adjacent ports should be perfectly isolated from each other. That is if port 1 is fed with a signal, the isolation losses at ports 2 and 4 should be zero, which in turn allows signal to pass through port 3. Figure 3.5 presents the scattering parameters of the designed crossover when port 1 is excited.

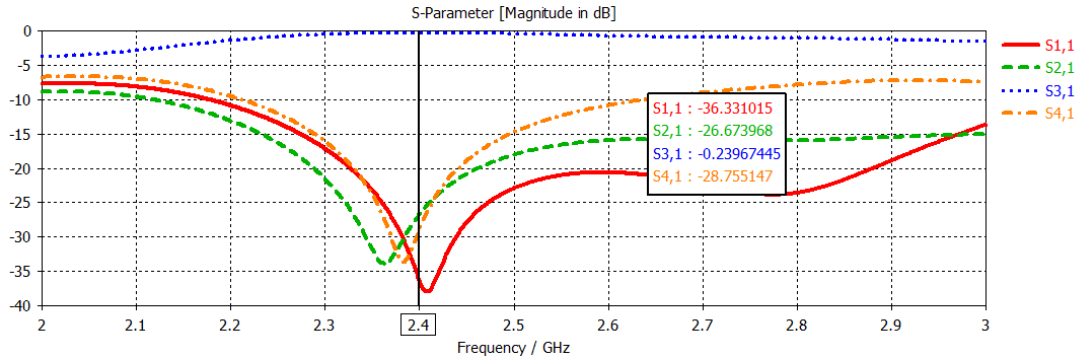

Figure 3.5: Crossover return, isolation, and insertion losses.

The isolation S_{21} between port 1 and port 2 was about -27dB where the isolation S_{41} between the ports 1 and 4 approximately, -29dB. These achievements exhibit a very good isolation results that prevent the signal to pass through the specified ports when port 1 is fed. In addition, the return loss S_{11} was about -36dB which shows an acceptable matching nearby the operating frequency. This means that there is no reflected signal to the input port side; all the power will be passed just from port 3, which is clear from coupling factor S_{31} that was exactly -0.23dB.

3.2.3 Phase Shifter

Phase shifters are used to delay the signal with a certain degrees of phase shifts. In this work, 45° phase shifter will be used by adding extra limited lengths Δl to the transmission line to provide 45° phase shift. Table 3.3 shows the dimensions for the added lengths shown in Figure 3.6.

Table 3.3: Phase shifter parameters.

Parameter	Value
f_r	2.4 GHz
ε_r	2.2
h	1.6 mm
$W_{(50\Omega)}$	4.9 mm
$\varepsilon_{eff(50\Omega)}$	1.87
$l_{(50\Omega)}$	15 mm
Δl	11.42 mm

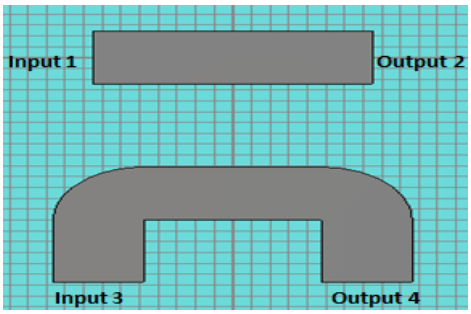

Figure 3.6: Phase shifter with added lengths.

In Figure 3.6, two microstrip transmission lines are simulated by using CST SUITE STUDIO. The input ports are port 1 and port 3, while the output phase shift must be measured at ports 2 and 4 respectively. Figure 3.7 shows the phase shift between the output ports when port 1 and port 3 were excited.

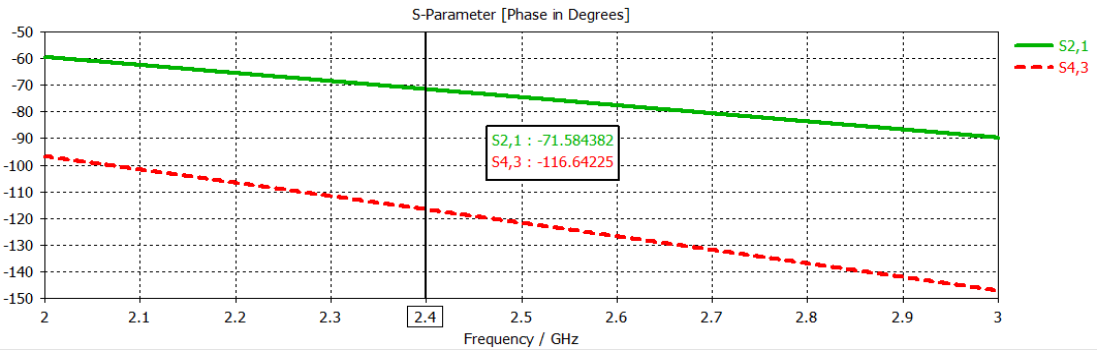

Figure 3.7: Measured phase shift at ports 2 and 4 when ports 1 and 3 fed.

To achieve the required phase shift, Δl line is divided and combined symmetrically between port 3 and port 4 as shown in Figure 3.6. The phase difference between the phase shifter output and the straight transmission line output when port 1 and port 3 is fed is about 45°. The phase shifter has good performance in terms of required phase shift.

3.2.4 Design and Simulation Results of 4×4 Conventional BM

3.2.4.1 Introduction

The BM components had been successfully designed and simulated. The performance of each component is guaranteed with the theoretical calculations. In this section, a BM components are combined to obtain a full design of BM.

3.2.4.2 Design and Simulation Results

Figure 3.8 shows a complete design of 4×4 BM, which consists of 4 hybrid couplers, two phase shifters and two crossovers. The input ports of BM are ports 1, 2, 3 and 4 where the output ports of BM are ports 5, 6, 7 and 8.

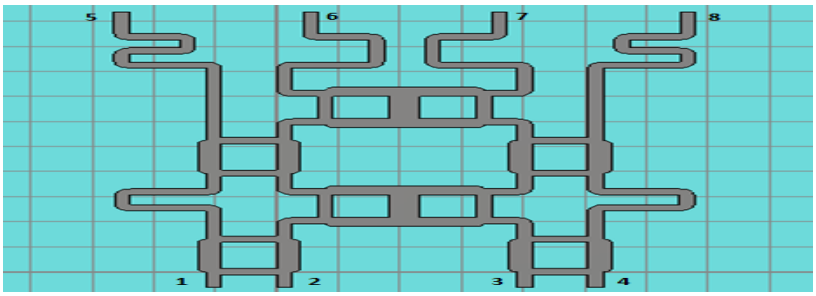

Figure 3.8: 4×4 conventional BM.

Then, each port is excited individually such that the return, isolation and insertion losses among BM are obtained from the scattering parameters of BM. Moreover, the phase shift between output ports when each input port fed individually can also be introduced from scattering parameters, as shown in Figure 3.9.

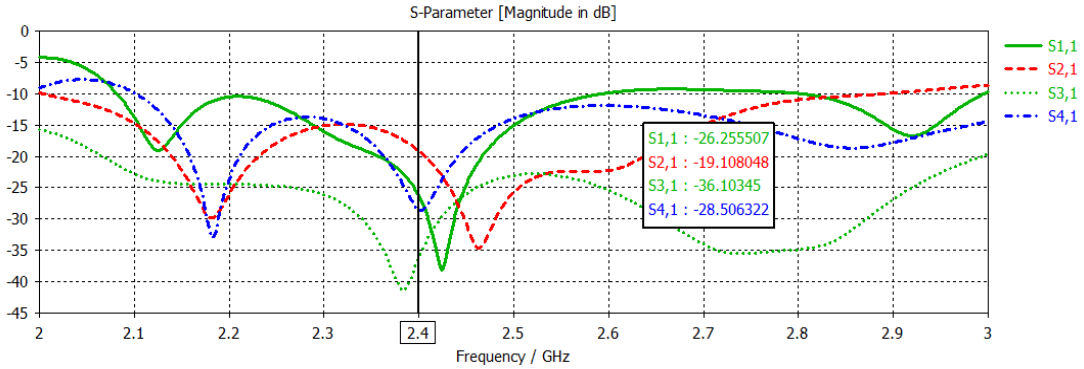

(a): Return and isolation losses when port 1 is fed.

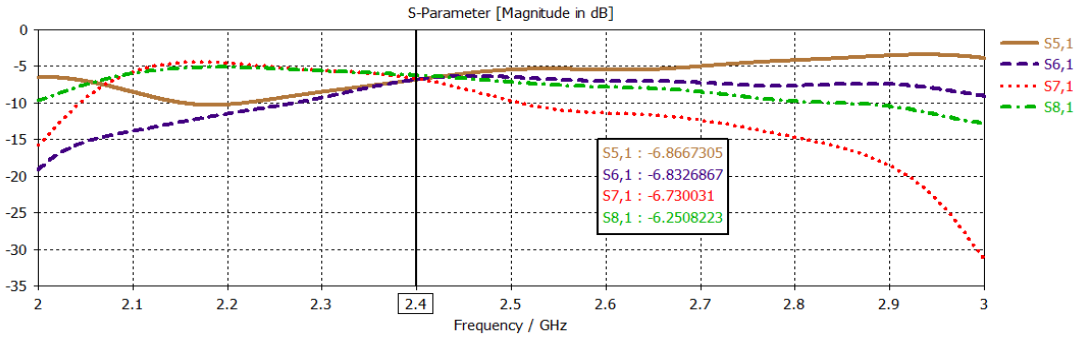

(b): Insertion losses when port 1 is fed.

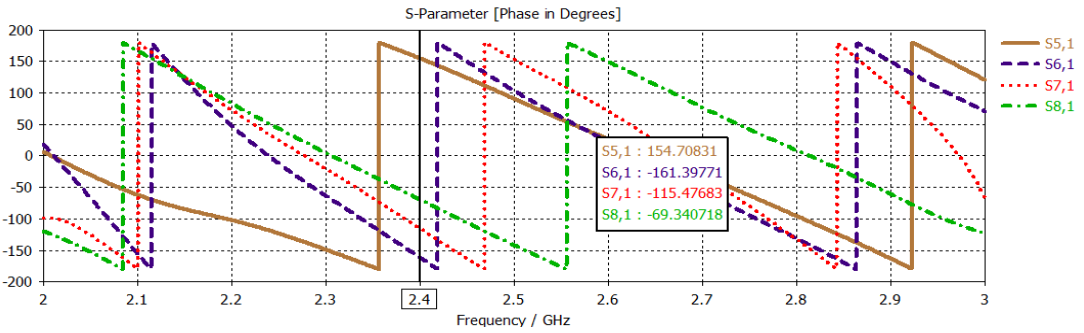

(c): Phase distribution of the output ports when port 1 is fed.

When port 1 is excited, the return loss S_{11} is around -26.2dB, which means that there is no reflected power to the input port side (i.e, matched port at 2.4 GHz). The insertion losses S_{51}, S_{61}, S_{71} and S_{81} are fluctuating between -6dB and -7dB due to losses in microstrip lines. The phase difference between output ports of BM when port 1 is fed is 45.32°, which is matched with theoretical calculations. Table 3.4 represents the losses values when port 1 is fed.

Table 3.4: The insertion losses, return and isolation when port 1 is fed.

Input Port 1	Return Loss (dB)	Isolation Losses (dB)			Insertion Losses (dB)			
S_{ij}	1	2	3	4	5	6	7	8
	-26.2	**-19.1**	**-36.1**	**-28.5**	**-6.8**	**-6.8**	**-6.7**	**-6.3**

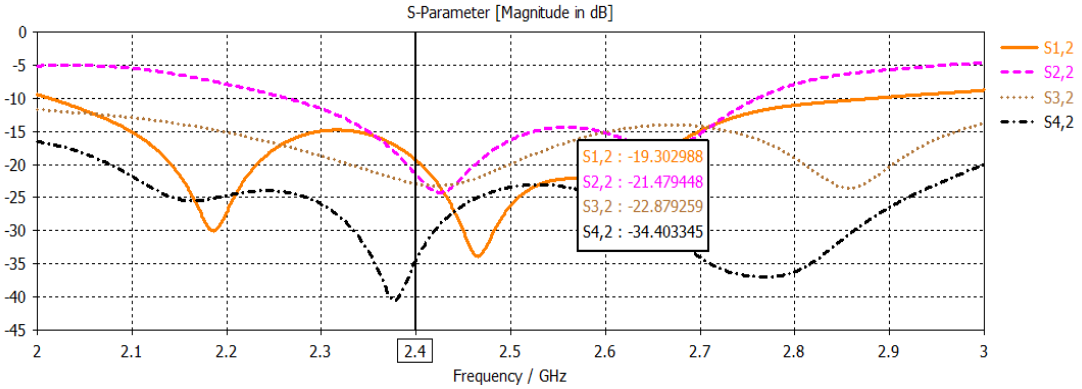

(d): Return and isolation losses when port 2 is fed.

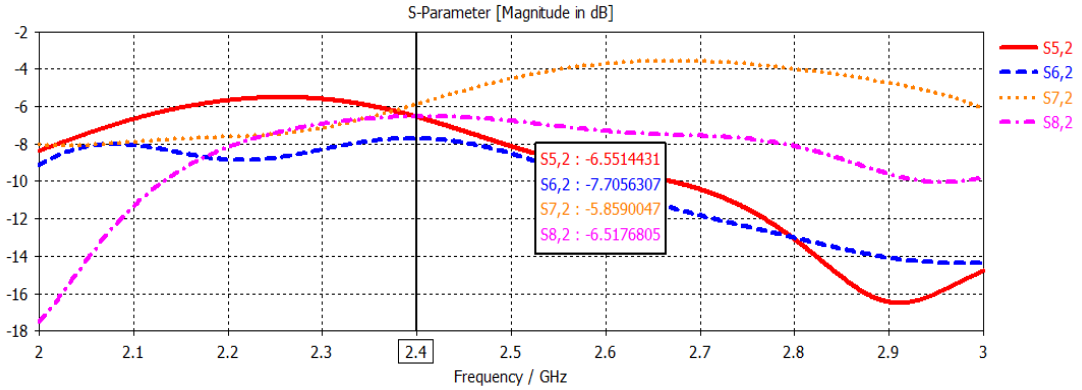

(e): Insertion losses when port 2 is fed.

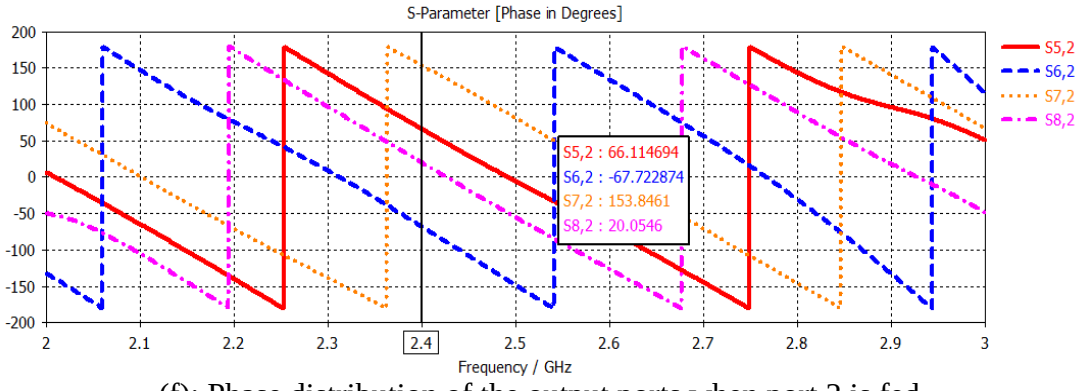

(f): Phase distribution of the output ports when port 2 is fed.

Different types of losses is obtained when port 2 is excited. The feeding port is matched based on the value of return loss S_{22} which is below -10dB. In terms of insertion losses, the values are fluctuating around -6dB due to insertion losses of microwave components. The phase difference between output ports of BM is about -135.35°, which assures the theoretical part which is mentioned in chapter 1. Table 3.5 represents different type of losses when port 2 is fed.

Table 3.5: The insertion losses, return and isolation when port 2 is fed.

Input Port 2	Return Loss (dB)	Isolation Losses (dB)			Insertion Losses (dB)			
S_{ij}	2	1	3	4	5	6	7	8
	-21.5	**-19.3**	**-22.9**	**-34.4**	**-6.6**	**-7.7**	**-5.8**	**-6.5**

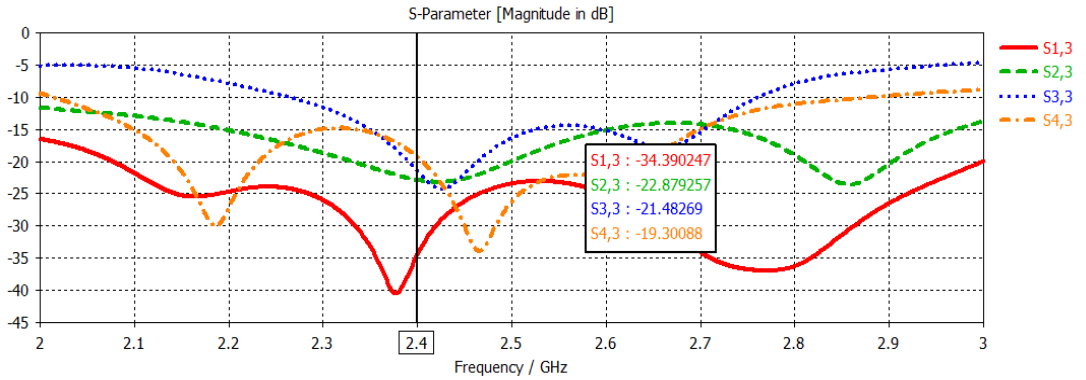

(g): Return and isolation losses when port 3 is fed.

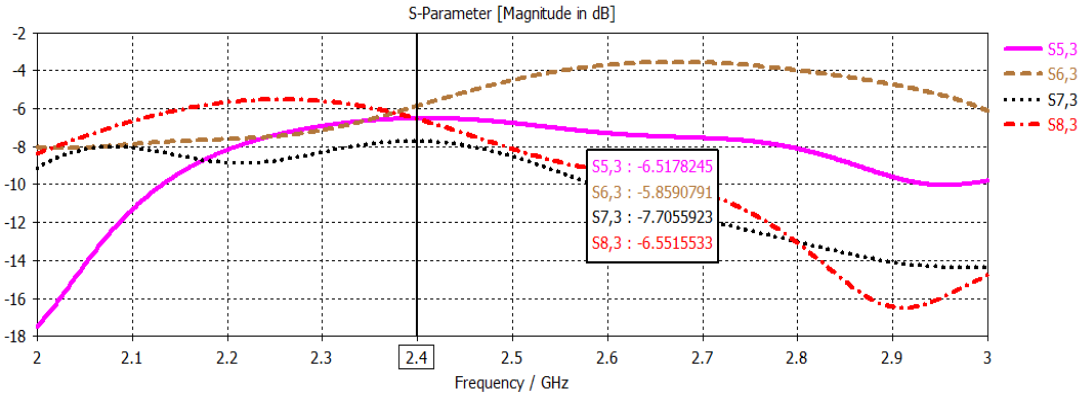

(h): Insertion losses when port 3 is fed.

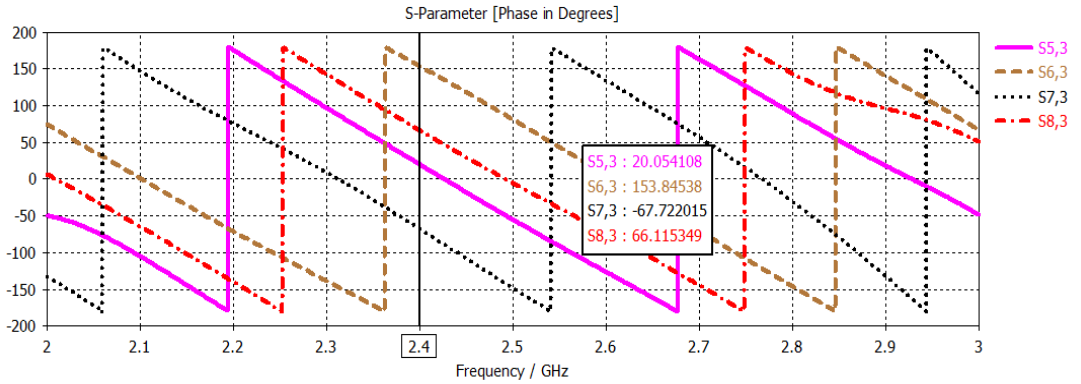

(i): Phase distribution of the output ports in case of port 3 is fed.

When the third port is considered as an excitation port, the return loss S_{33} hits -21.4dB. This value assure that there is no reflected power toward the input port side; most of power will be passed through port 3. The insertion losses have acceptable fluctuating values around -6dB while the phase difference between output ports are about 135.35°. These results are presented in Table 3.6.

Table 3.6: The insertion losses, return and isolation when port 3 is fed.

Input Port 3	Return Loss (dB)	Isolation Losses (dB)			Insertion Losses (dB)			
S_{ij}	3	1	2	4	5	6	7	8
	-21.5	**-34.4**	**-22.9**	**-19.3**	**-6.5**	**-5.8**	**-7.7**	**-6.6**

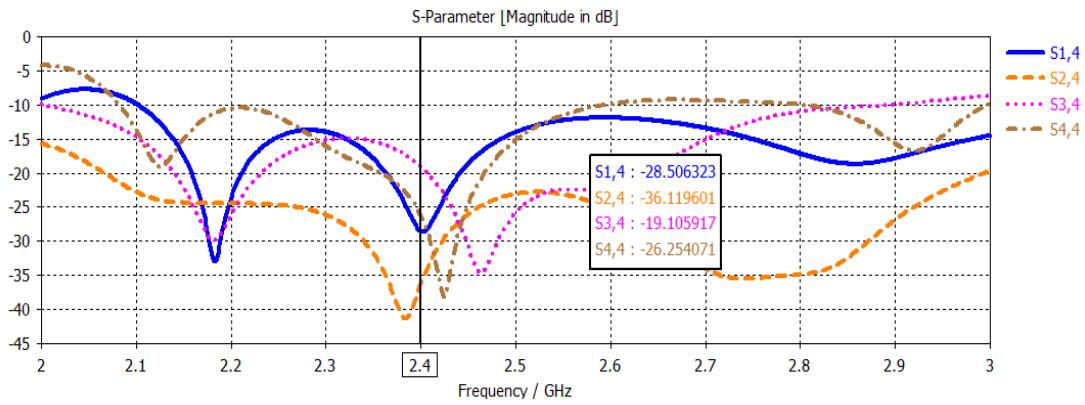

(j): Return and isolation losses when port 4 is fed.

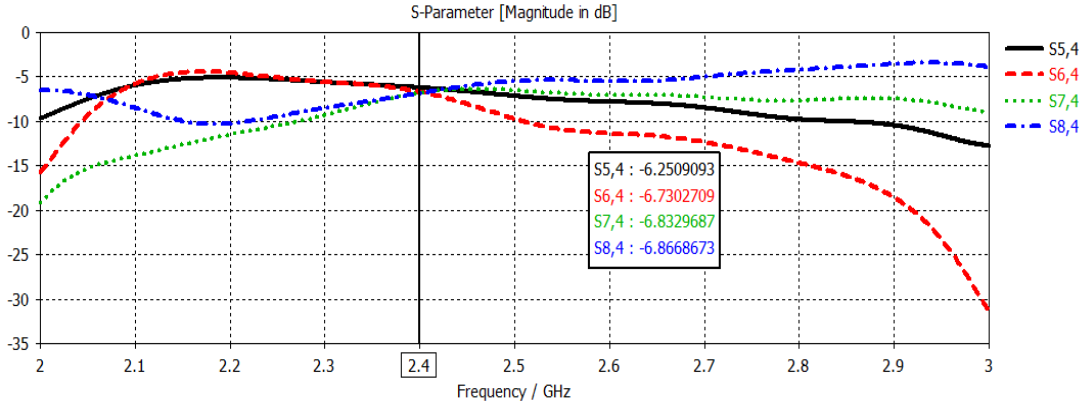

(k): Insertion losses when port 4 is fed.

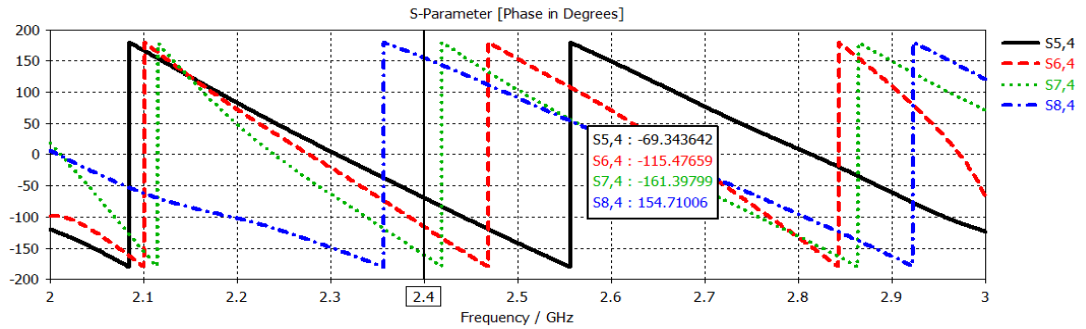

(l): Phase distribution of the output ports in case of port 4 is fed.

Figure 3.9: Return losses, isolation losses, insertion losses and phase shift at each output port when different input ports are fed.

Finally, port 4 is the input port. The return loss S44 is below -10dB which assures matching at the operating frequency. The insertion losses is roughly -6dB as shown in Table 3.7 where the phase difference at the output of BM is around -45.32°.

Table 3.7: The insertion losses, return and isolation when port 4 is fed.

Input Port 4	Return Loss (dB)	Isolation Losses (dB)			Insertion Losses (dB)			
S_{ij}	4	1	2	3	5	6	7	8
	-26.2	**-28.5**	**-36.1**	**-19.1**	**-6.3**	**-6.7**	**-6.8**	**-6.8**

As shown in Figure 3.9, a very good matching between simulated and theoretical measurements had been presented. The power at the output ports is divided equally

(about – 6dB) when each input port was fed individually. On the other hand, a very good isolation and return losses is obtained as shown in Figure 3.9. In terms of phase shifts, an acceptable phase shift difference between adjacent output ports is obtained. Tables 3.8 summarizes the phase difference between output ports of BM when different input ports are excited.

Table 3.8: Phase shift between different ports of the BM.

Output Ports / Input Ports	Port 5	Port 6	Port 7	Port 8	φ average
Port 1	154.70°	-161.39°	-115.47°	-69.34°	45.32°
Port 2	66.11°	-67.72°	153.85°	20.05°	-135.35°
Port 3	20.05°	153.85°	-67.72°	66.11°	135.35°
Port 4	-69.34°	-115.47°	-161.39°	154.71°	-45.32°

3.2.5 Patch Antenna Design and Simulation Results

In the previous sections, the BM is successfully designed and simulated; it had a very good performance in terms of phase shift and different types of losses. Now, patch antenna array consists of four elements that must be combined at the output of BM. In the following section, a design and simulated results of a single rectangular patch antenna with its radiation characteristics is illustrated.

3.2.5.1 Single Patch Antenna Design and Simulation Results

Figure 3.10 shows the single element rectangular patch antenna fed by inset feed line technique. The dimensions of the parameters are given by Table 3.9. The antenna is designed with Roger RT 5880 having 2.2 relative permittivity and operates at 2.4 GHz. The following equations are used to obtain the length and width of the rectangular patch antenna.

$$W_p = \frac{C}{2f_r}\sqrt{\frac{2}{\varepsilon_r + 1}} \tag{3.6}$$

$$\Delta L = 0.412h\,\frac{(\varepsilon_{eff} + 0.3)\left(\frac{W}{h} + 0.264\right)}{(\varepsilon_{eff} - 0.258)\left(\frac{W}{h} + 0.8\right)} \tag{3.7}$$

$$L_{eff} = \frac{C}{fr\sqrt{\varepsilon_{eff}}} \tag{3.8}$$

$$L_p = L_{eff} - 2\Delta L \tag{3.9}$$

Moreover; the inset feed line dimension can be calculated using the following formula

$$Zo = R_{in}\,cos^2\left(\frac{\pi}{Lp}y\right) \tag{3.10}$$

Where;

W_p: Patch Width

L_p: Patch Length

L_{eff}: Effective Patch length

ΔL: Enlargement on Lp due to fringing field effects.

R_{in}: The resonant input resistance when the patch is fed at a radiating edge

y: Inset distance from the radiating edge which is selected such that Zo is equivalent to the feed line impedance.

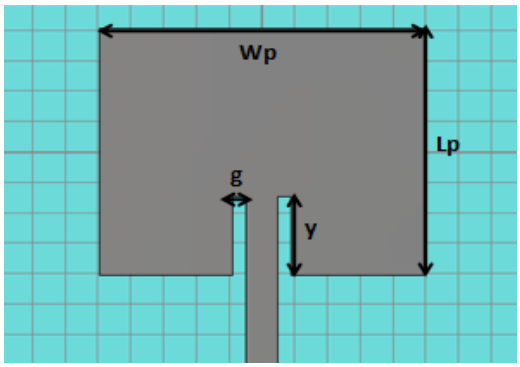

Figure 3.10: Designed single patch antenna.

Table 3.9: Single patch parameter with dimensions.

Parameter	Value
f_r	2.4 GHz
ε_r	2.2
h	1.6 mm
W_p	49.41 mm
L_p	40.75 mm
y	13 mm
g	2 mm

The return loss and radiation pattern of the simulated patch antenna are shown in Figures 3.11 and 3.12 respectively. It is clear that the rectangular patch antenna has a very good matching around resonant frequency, since the return loss S_{11} is below -10dB. The radiation pattern can also describe the antenna performance; the directivity is shown in polar coordinate system to show the beam pattern shape. At 2.4 GHz, the directivity hits the peak at 7.79dBi while the SLL reached to -19.4dB. Table 3.10 summarizes the performance and characteristics of a single patch antenna operating at 2.4 GHz.

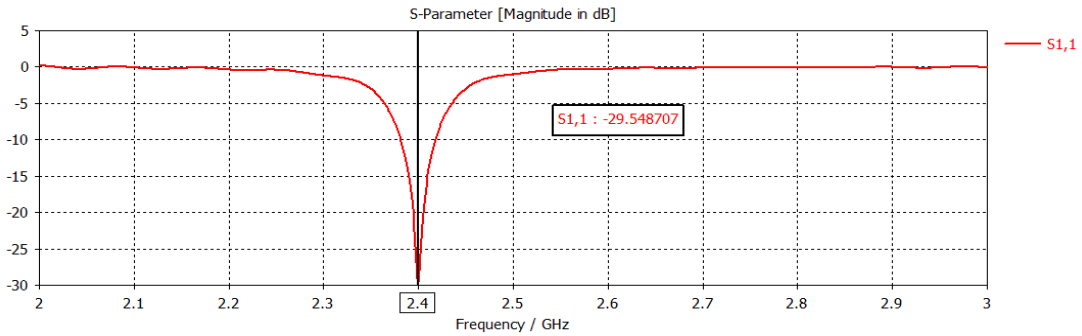

Figure 3.11: Patch antenna return Loss.

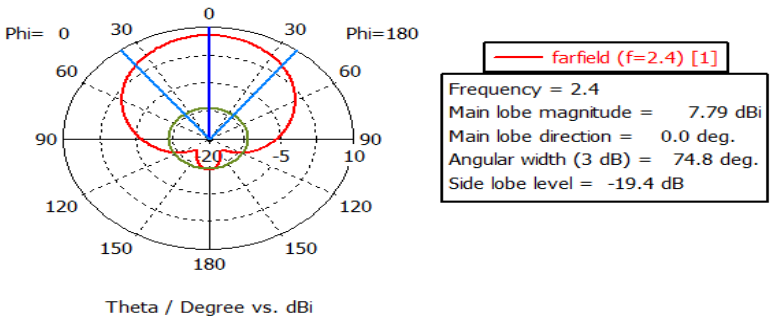

Figure 3.12: Radiation pattern of patch antenna.

Table 3.10: Patch antenna performance and characteristics.

S11	Directivity	Gain	SLL	HPBW	BW
-29.5 dB	7.79 dBi	7.52 dB	-19.4 dB	74.8°	36.6 MHz

3.2.6 Phased Antenna Array Based on 4×4 BM

In this section, a combination between antenna array consisting of four elements of previously designed rectangular patch antenna with 4×4 BM based on microstrip technology, as shown in Figure 3.13. The spacing between antenna elements are half wave length in order to obtain the desired radiation pattern when different input ports are fed.

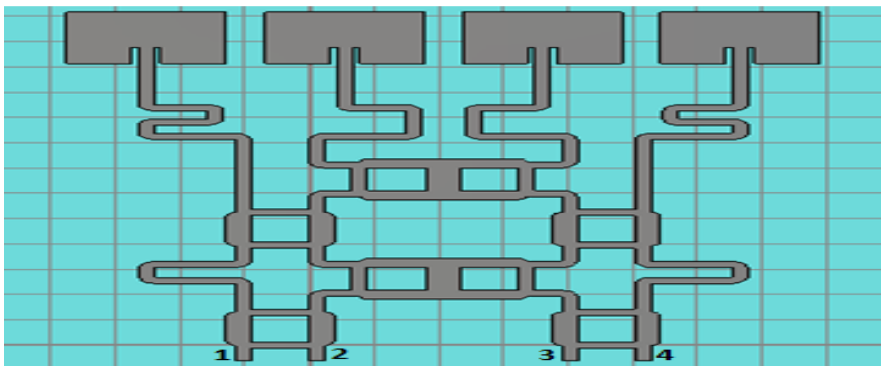

Figure 3.13: Phased antenna array using 4×4 BM.

Four orthogonal radiation patterns are obtained by exciting the input ports individually. Figures 3.14 and3.15 show the radiation patterns in Cartesian coordinate system when the signal is fed from ports 1 and 4.

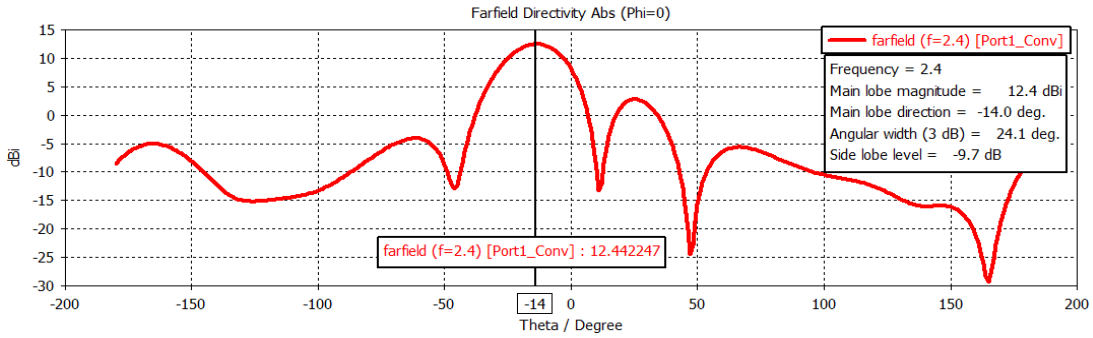

Figure 3.14: Radiation pattern of the conventional structure when port 1 is fed.

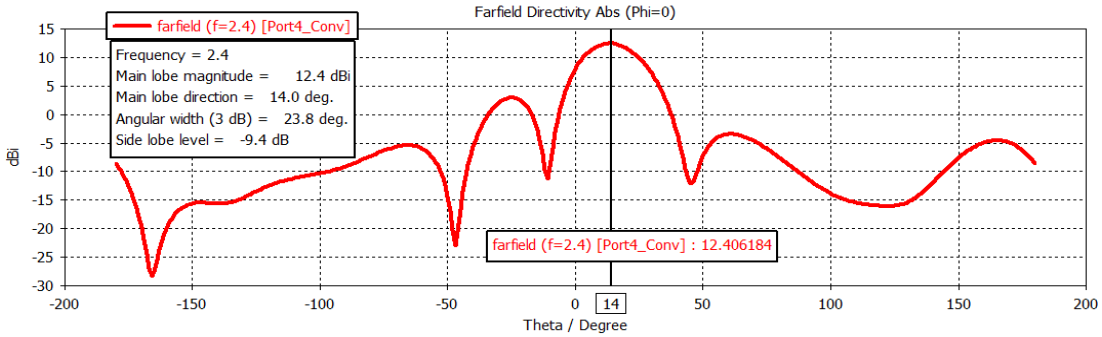

Figure 3.15: Radiation pattern of the conventional structure when port 4 is fed.

Figures 3.14 and 3.15 illustrate that the main beam directions are -14° and 14° when the signal was excited from ports 1 and 4 respectively. The main beam has narrower BW comparing it with single element patch antenna. Moreover, high directivity was obtained when the first and last ports were fed. Therefore, a very directive pattern with minimum side lobe levels can be obtained. On the other hand, Figures 3.16 and 3.17 show the radiation patterns when the signal is fed from ports 2 and 3 individually.

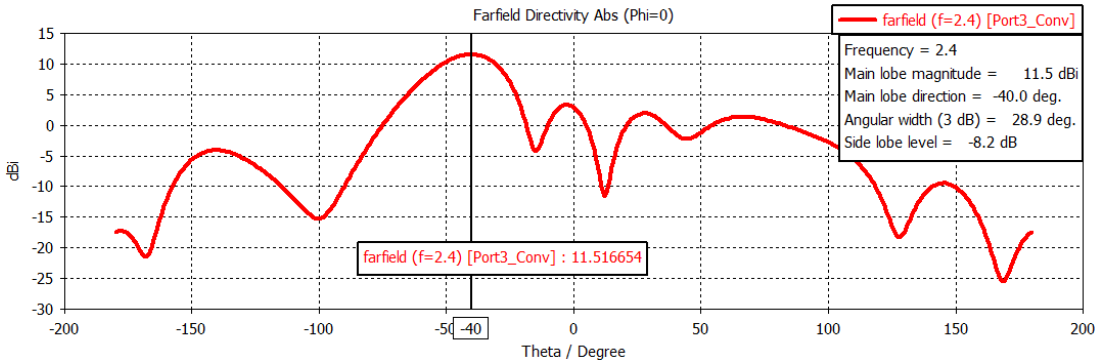

Figure 3.16: Radiation pattern of the conventional structure when port 2 is fed.

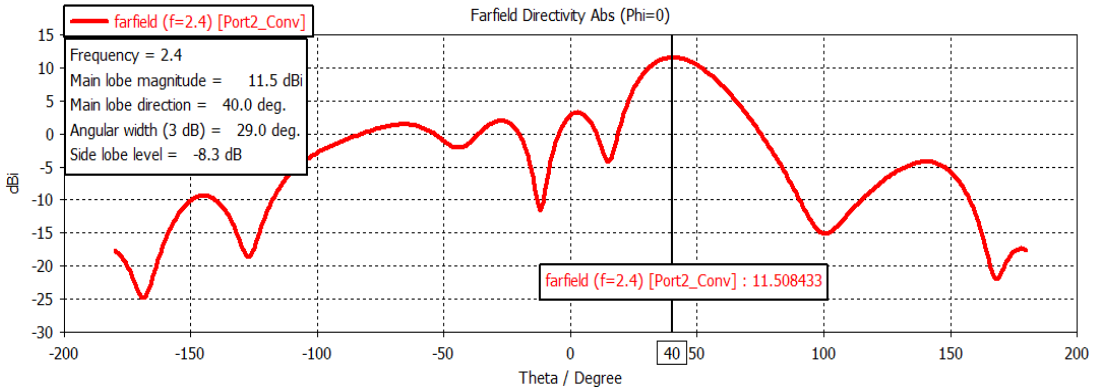

Figure 3.17: Radiation pattern of the conventional structure when port 3 is fed.

The main beam is switched to 40° and -40° when the input signal is fed from ports 2 and 3 respectively. They have the same characteristics except the direction of the main lobe while the directivity is about 11.5dBi with acceptable side lobe levels. Moreover, a narrower BW is obtained in each case of feeding.

The design and simulation of phased antenna array based on 4×4 conventional BM was successfully achieved for 2.4 GHz applications. It is important to see the four main beams together to check the covering range at the operating frequency. Figure 3.18 introduce the beams in -14°, 40°, -40° and 14° in Cartesian plot for different excitation ports.

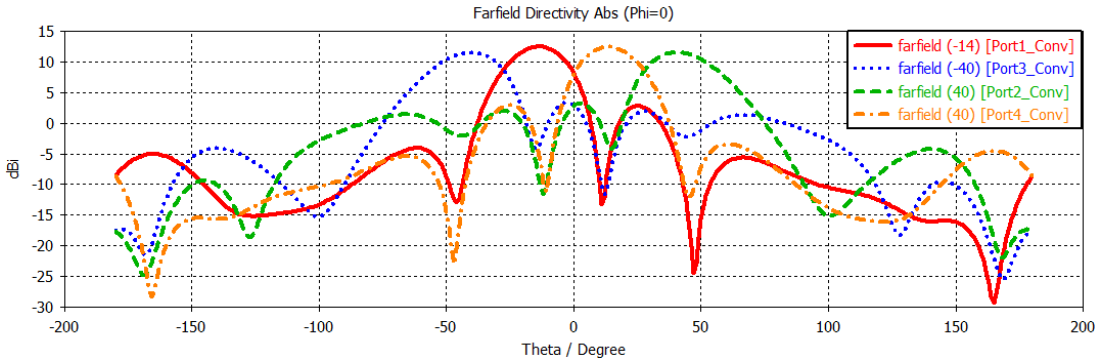

Figure 3.18: Four radiation patterns when different input ports were applied in Cartesian coordinate system.

The spatial scan coverage was about 106.8°, which means that this kind of SBS can detect the target among the mentioned range. The simulation results of phased microstrip antenna array based on microstrip BM are summarized in Table 3.11 which shows the system physical size, directivity of antenna array, spatial scan coverage, scanning angles, and SLL's when different input ports is excited by a signal.

Table 3.11: Phased antenna array based on BM.

Features	**Phased Antenna Array using B.M**
Center Frequency	2.4 GHz
Physical Size	27cm×23cm
Antenna Directivity: $\boldsymbol{\varphi = \pm 45}$ $\boldsymbol{\varphi = \pm 135}$	 12.4 dBi 11.5 dBi
Spatial Scan Coverage	106.8°
Maximum scan angle: $\boldsymbol{\varphi = \pm 45}$ $\boldsymbol{\varphi = \pm 135}$	 ±14° ±40°
SLL: $\boldsymbol{\varphi = \pm 45}$ $\boldsymbol{\varphi = \pm 135}$	 -9.4 dB -8.2 dB

3.3 Analysis and Design of Modified BM

3.3.1 Introduction

The strip line has two homogeneous dielectric substrates. Theoretically, the substrate is extended from -∞ to ∞, but the strip line fields will not extend far away from the center of conductor, and hence the geometry of strip line structure can be simplified by truncating the plates beyond some distance near to the edges of conductors.

In this section, a strip line technology will be used instead of a microstrip line technology as a feeding network to form a BM. The reason of using this technique is to reduce the radiation loss at the edges and discontinuities of the microwave feeding circuit, which appears as long as the microstrip feeding network is used, in turns disturbs the pattern of the integrated antennas at the output ports of BM and increases the SLL's. This method of feeding is called a proximity coupling technique, which was mentioned in chapter 2. In order to form an antenna array, square slots are punctured to deploy the array on the upper ground plane layer. The feeding network consists of 3-dB quadrature coupler, crossover and 45° phase shifter will be designed based on the strip line technology, having the same substrate layer properties in terms of the substrate permittivity and conductivity as shown in the coming subsections.

Figures 3.19 and 3.20 show microstrip and strip line. The strip line consists of two ground planes in the above and lower layers while the substrate is printed between them. The strip line is located in the middle of substrate layer as shown in Figure 3.20. The objective is to select the appropriate line technology to be used for the implementation of the feeding network of phased antenna array based on BM. The radiation tests were carried out by using CST SUIT STUDIO on both lines.

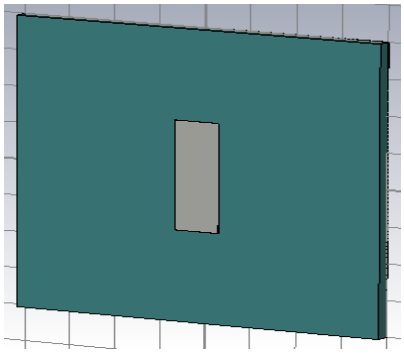

Figure 3.19: Microstrip line

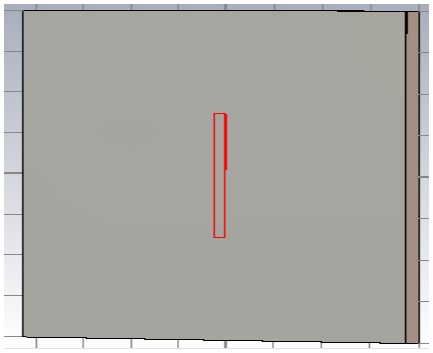

Figure 3.20: Strip Line

Figure 3.21 shows the simulation results of microstrip and strip lines. It is obvious that the radiation loss is decreased when a strip line technology is used, especially in the vertical direction. Based on these results, it is expected that the BM based on the strip line technology will be better than BM based on microstrip technology in terms of radiation loss, because the effect of radiation of strip line is less compared to microstrip line and hence, the antenna array radiation pattern will not be affected from the superior's radiation due to the feed network.

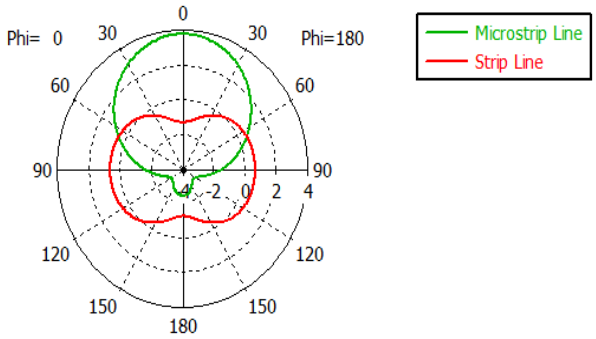

Figure 3.21: Microstrip and strip line radiation test

3.3.2 3-dB Coupler Design and Simulation Results Using Strip Line Technique

The 3-dB strip line coupler consists of main of 50Ω line, which is coupled to two secondary lines having an impedance of 35.35Ω and a length of quarter wave length. The dimensions of the strip line can be calculated based on the following formulas:

$$Zo = \frac{30\pi}{\sqrt{\varepsilon_r}} \frac{b}{(W_e + 0.441b)} \tag{3.11}$$

where b is the overall substrate thickness and W_e is the effective width of the center conductor which is given by Equation 3.12:

$$\frac{W_e}{b} = \frac{W}{b} - \begin{cases} 0, & for\ \frac{W}{b} > 0.35 \\ (0.35 - (W/b))^2, & for\ \frac{W}{b} < 0.35 \end{cases} \tag{3.12}$$

During the design of strip lines, one usually needs to find the width of the strip line based on Equation 3.13:

$$\frac{W}{b} = \begin{cases} x & , for\ \sqrt{\varepsilon_r} Zo < 120 \\ 0.85 - \sqrt{0.6 - x}, & for\ \sqrt{\varepsilon_r} Zo > 120 \end{cases} \tag{3.13}$$

where;

$$x = \frac{30\pi}{\sqrt{\varepsilon_r}\, Zo} - 0.441 \tag{3.14}$$

Based on strip the line formulas, it is easy to obtain the coupler dimensions. Table 3.12 presents the 3-dB coupler dimensions, which are illustrated in Figure 3.22.

Table 3.12: Coupler parameters based on strip line technology.

Parameter	Value
$\boldsymbol{f_r}$	2.4 GHz
$\boldsymbol{\varepsilon_r}$	2.2
$\boldsymbol{h_1}$	0.8 mm
$\boldsymbol{h_2}$	0.8 mm
$\boldsymbol{W_{(50\Omega)}}$	1.2 mm
$\boldsymbol{W_{(35.35\Omega)}}$	2.07 mm
$\boldsymbol{\lambda_{g(50\Omega)}/_4}$	20.4 mm
$\boldsymbol{\lambda_{g(35.35\Omega)}/_4}$	20.4 mm

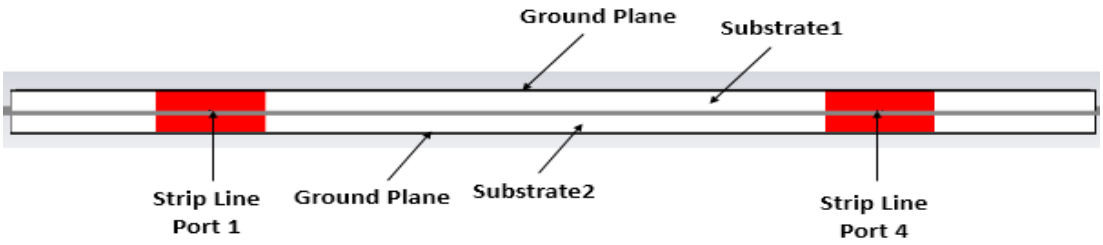

(a): Side view

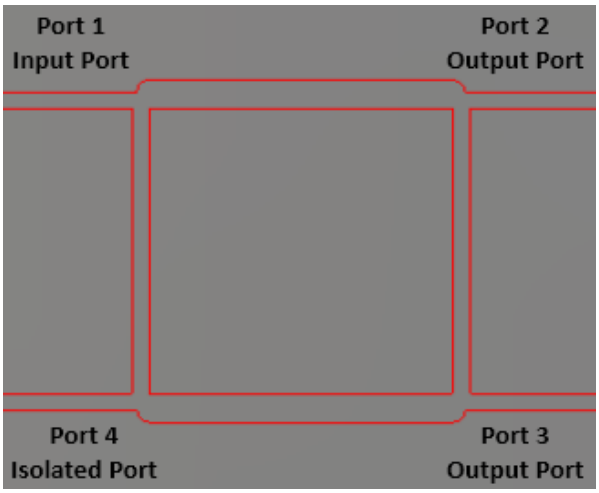

(b): Top view

Figure 3.22: 3-dB Coupler design, (a): side view, (b): top view.

The coupler performance can be determined according to its scattering parameters. Figure 3.23 shows the coupler scattering parameters.

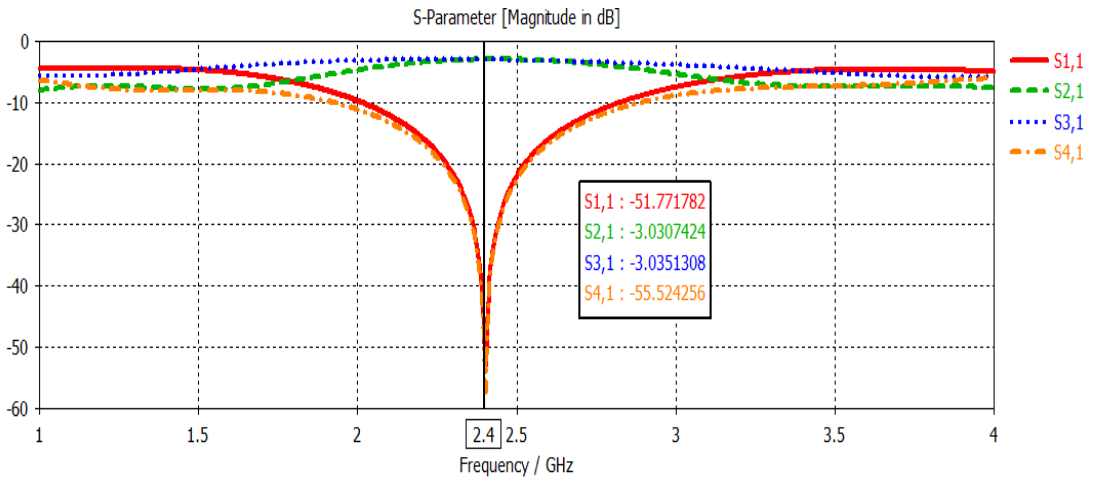

Figure 3.23: Scattering parameters of 3-dB coupler design.

In this design, the input port is port 1. The return loss shows that the designed coupler has better matching comparing with the conventional 3-dB hybrid coupler since S_{11} dropped to -51.7dB. On the other hand, port 4 is an isolated port (i.e. the isolation loss S_{41} hit -55.5dB) while the insertion losses are around -3dB which means that the power is equally divided between output ports.

In terms of the phase shift, Figure 3.24 shows that there is 90° difference in phase between ports 2 and 3 when port 1 is excited.

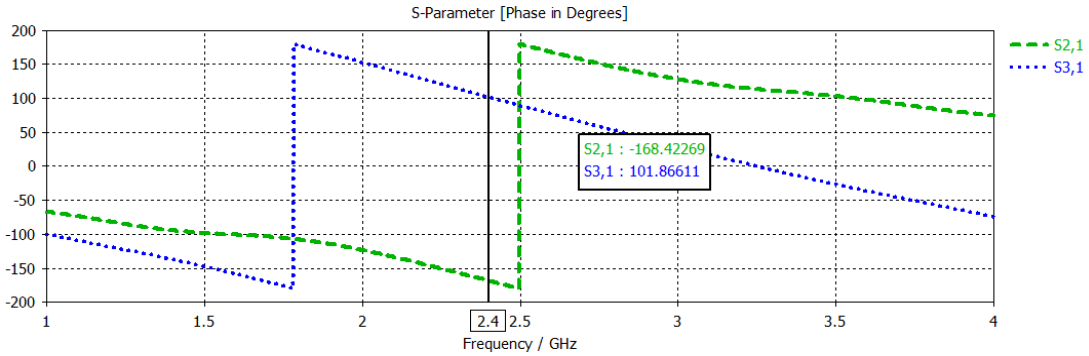

Figure 3.24: Phase shift at output ports.

3.3.3 Crossover Design and Simulation Results Based on the Strip Line Technology

Cascading two couplers designed by using strip line technology results in a crossover. The objective of this design is to obtain a very good isolation between the crossing lines. Table 3.13 shows the crossover design parameters while Figures 3.25.a and 3.25.b show the schematic diagrams of the designed crossover.

Table 3.13: Crossover parameters.

Parameter	Value
f_r	2.4 GHz
ε_r	2.2
h_1	0.8 mm
h_2	0.8 mm
$W_{(50\Omega)}$	1.2 mm
$W_{(35.35\Omega)}$	2.03 mm
$W_{(25\Omega)}$	3.17 mm
$\lambda_{g(50\Omega)}/_4$	21 mm
$\lambda_{g(35.35\Omega)}/_4$	21 mm

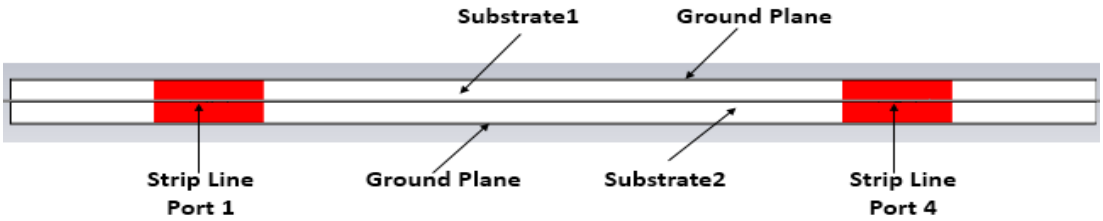

(a): Side view

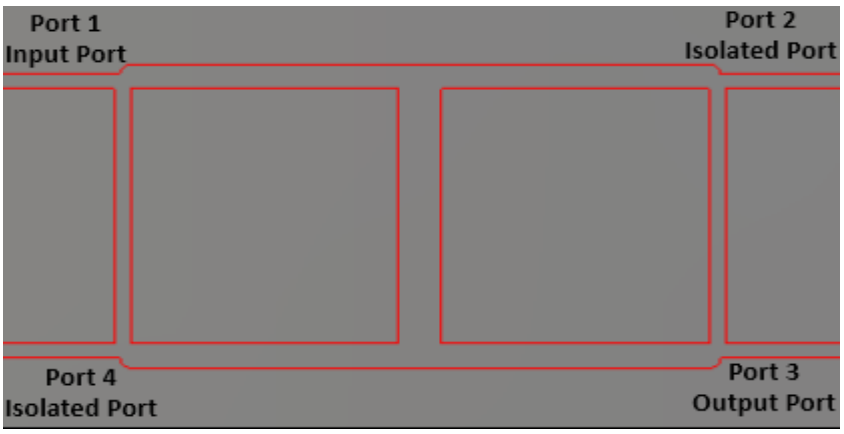

(b): Top view

Figure 3.25: Designed crossover, (a): side view, (b): top view.

Figure 3.26 presents the scattering parameters of the designed crossover when the input power was excited from port 1.

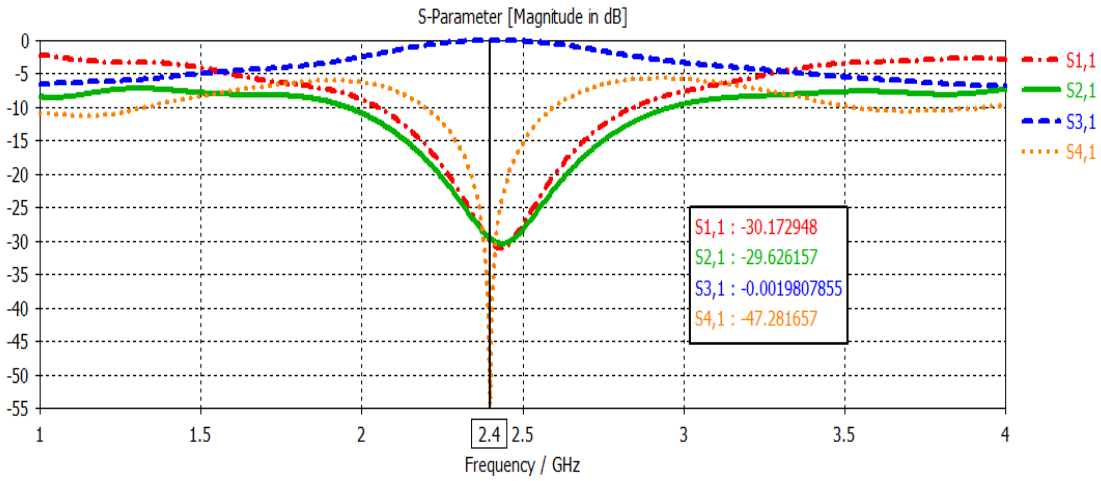

Figure 3.26: Scattering parameter of the designed crossover.

From Figure 3.23, the return loss hit -30 dB, which means that there is no power reflected to the input port side, in addition, ports 2 and 4 are perfectly isolated while port 3 is the output port.

3.3.4 Phase Shifter Based on Strip Line Technique

Adding extra length to the transmission line (microstrip or strip line) can change the phase shift between input and output ports. If port 1 is an input port and port 2 is the output port, then according to Equation 2.12, a specific length Δl can be added to obtain 45° phase shift between input and output ports. Table 3.14 represents the parametric dimensions of the designed phase shifter based on the strip line technology. Figures 3.27.a and 3.27.b show schematic diagrams of the designed phase shifter.

Table 3.14: 45° Phase shifter parameter.

Parameter	Value
f_r	2.4 GHz
ε_r	2.2
h_1	0.8 mm
h_2	0.8 mm
$W_{(50\Omega)}$	1.2 mm
$l_{(50\Omega)}$	21 mm
Δl	51.54 mm

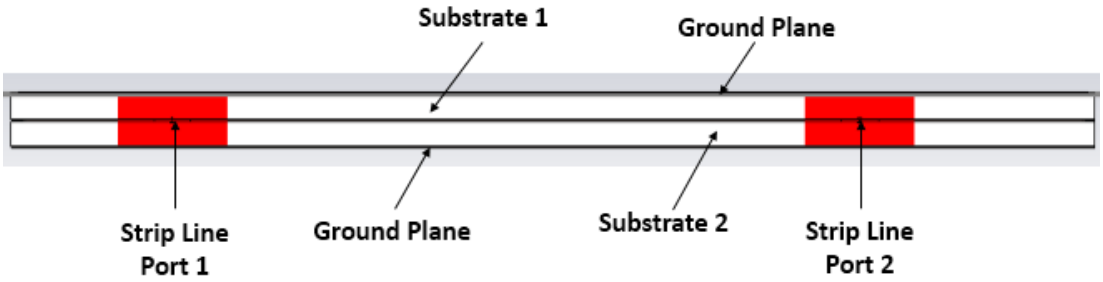

(a): Side view

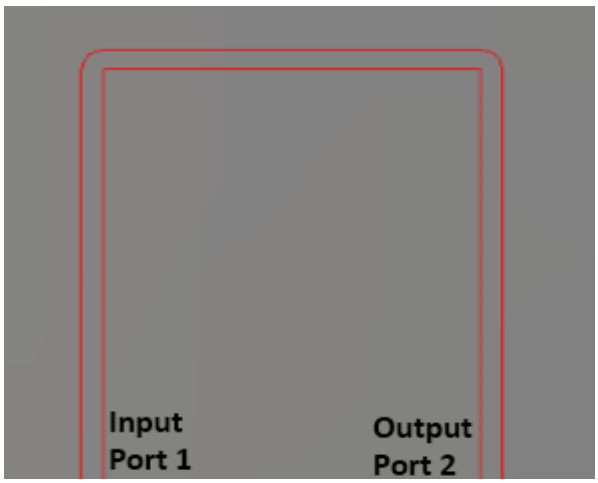

(b): Top view

Figure 3.27: 45° Phase Shifter design, (a): side view, (b): top view.

Figure 3.28, demonstrates the measured phase shift at the output port when the excitation port is port 1. The phase difference is about 45°.

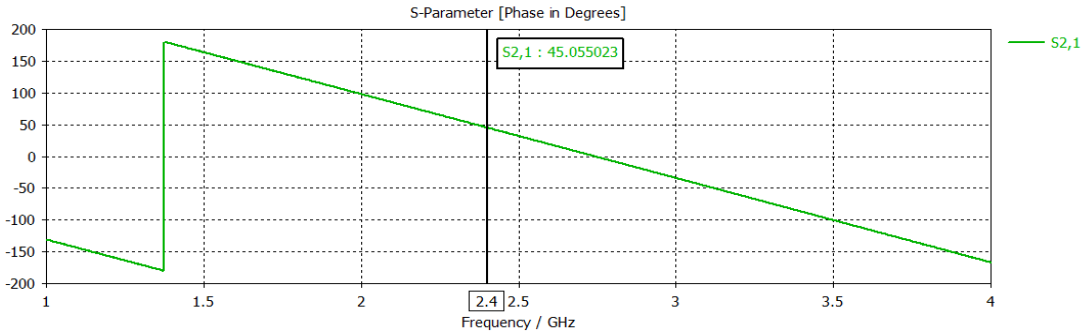

Figure 3.28: Phase shift at the output port of 45° phase shifter.

3.3.5 Design and Simulation Results of 4×4 Modified BM based on Strip Line Technique

3.3.5.1 Introduction

The three main parts of BM are successfully designed and simulated for 2.4 GHz applications. The next step is to combine BM components to get a feeding network based on strip line technique.

3.3.5.2 Design and Simulation Results

Figure 3.29 shows a complete design of 4×4 BM. It consists of four 3-dB couplers, two crossovers and two-phase shifters. The designs are carried out based on strip line technology. The input ports are 1, 2, 3, and 4 while the output ports are 5, 6, 7 and 8.

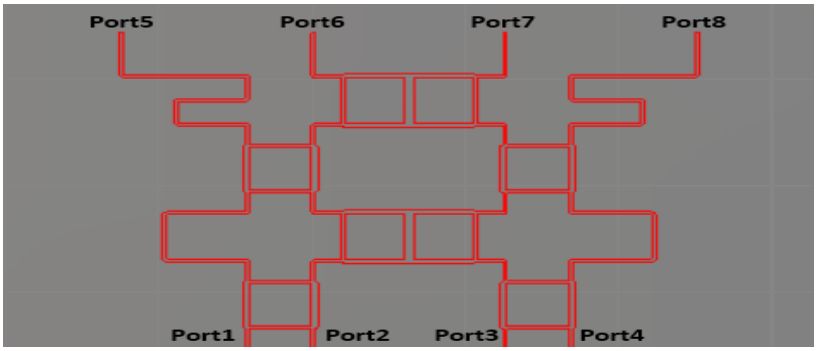

Figure 3.29: BM based on strip line technology.

Each input port is individually excited by the signal while the return, isolation and insertion losses are obtained at the output of BM. It is expected to get results close to

the theoretical calculations that mentioned in Chapter 1. The detailed simulation results are shown in Figure 3.30.

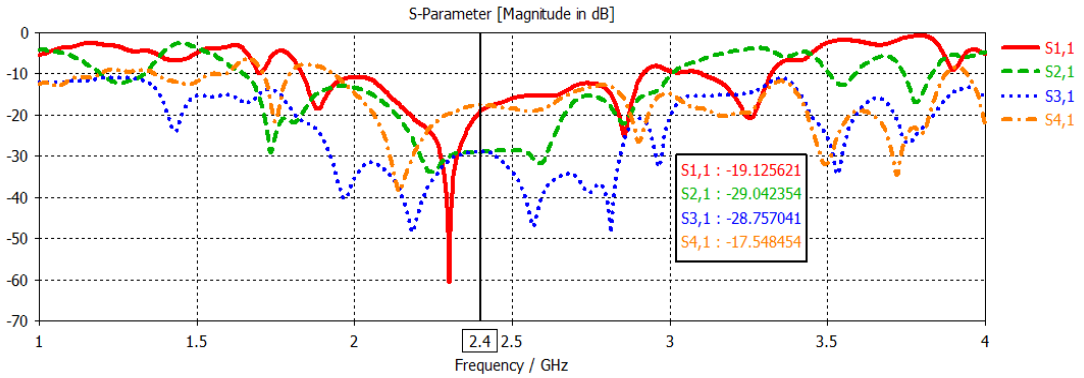

(a): Return and isolation losses when port 1 is fed.

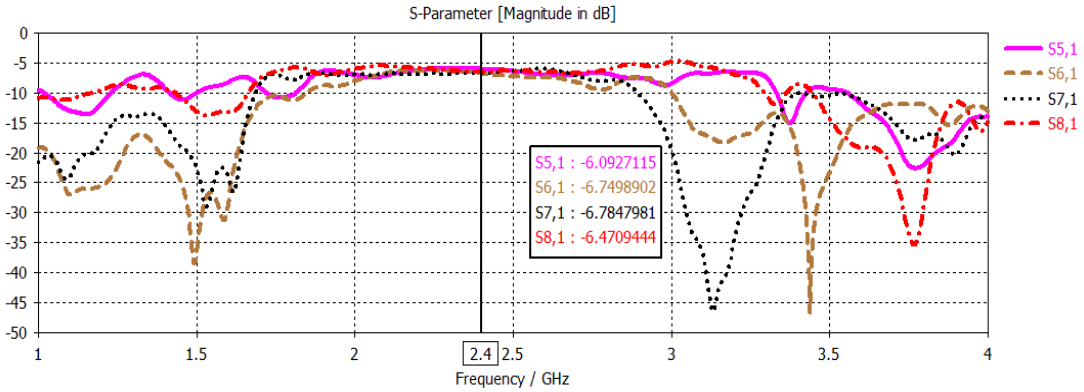

(b): Insertion losses when port 1 is fed.

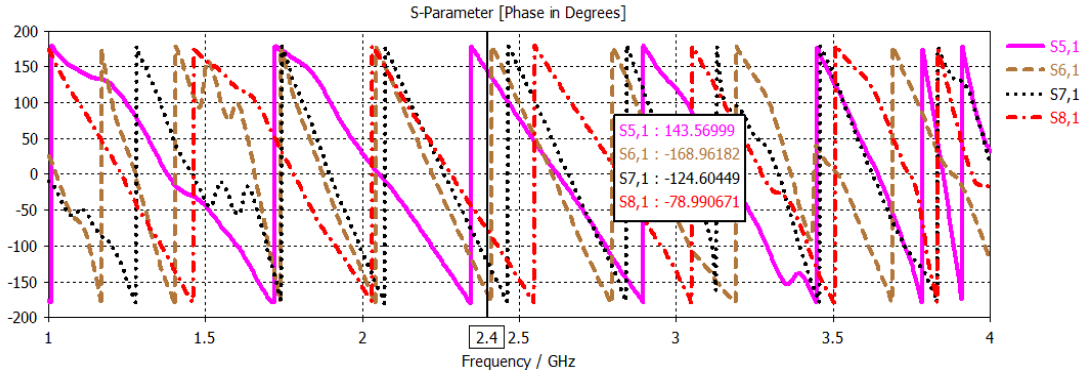

(c): Phase distribution of the output ports when port 1 is fed.

When port 1 is fed, the return loss S11 hits -19dB, that in turns achieve matching at the operating frequency, in addition, the insertion loss is around -6dB as expected. In terms of phase, a 45.7° average phase difference is achieved at the output of BM. Table 3.15 shows the simulation results when port 1 is excited.

Table 3.15: The insertion losses, return and isolation when port 1 is fed.

Input Port 1	Return Loss (dB)	Isolation Losses (dB)			Insertion Losses (dB)			
S_{ij}	1	2	3	4	5	6	7	8
	-19.1	**-29.0**	**-28.7**	**-17.5**	**-6.1**	**-6.7**	**-6.7**	**-6.4**

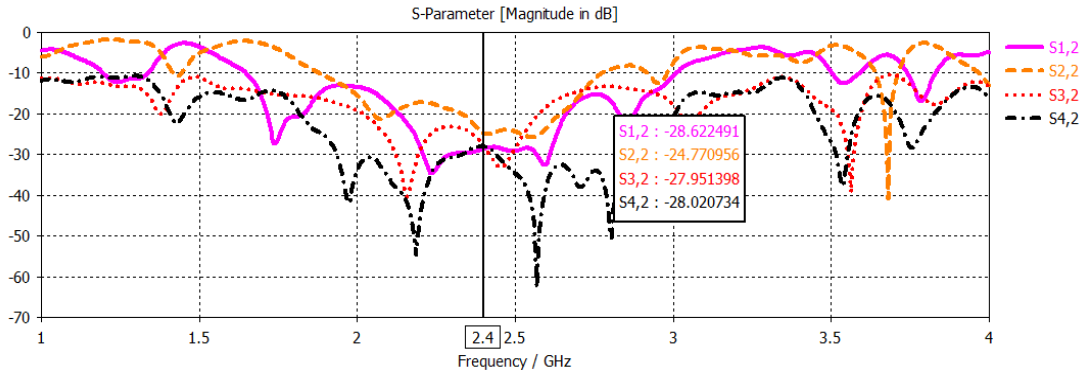

(d): Return and isolation losses when port 2 is fed.

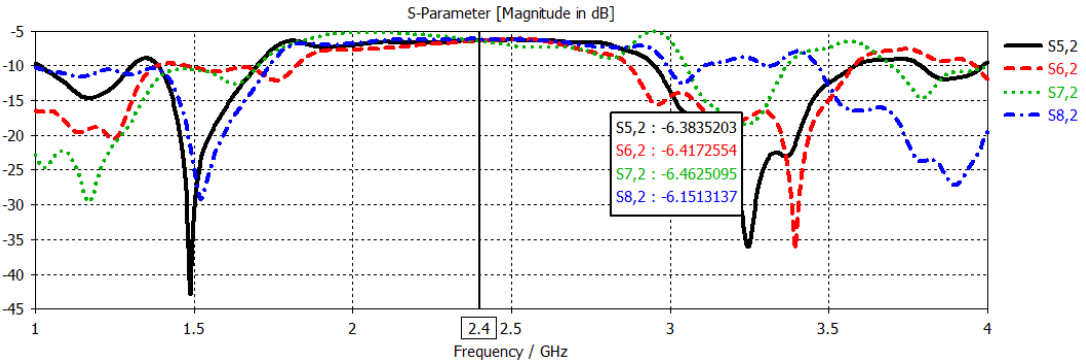

(e): Insertion losses when port 2 is fed.

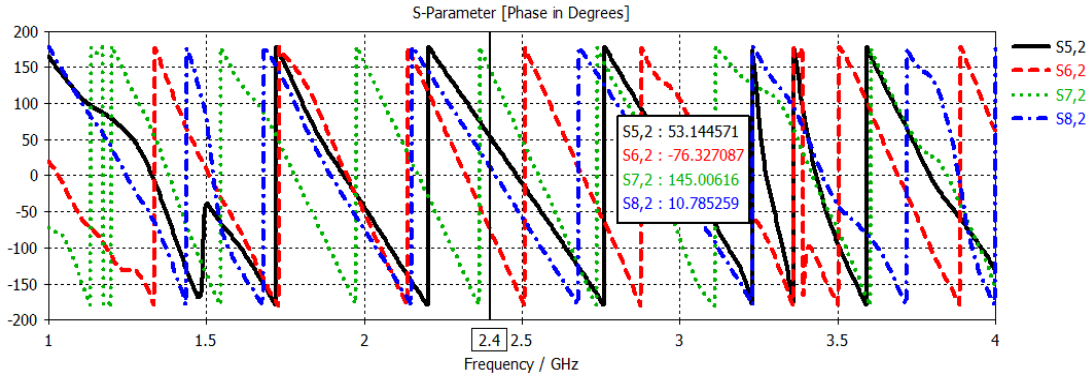

(f): Phase distribution of the output ports when port 2 is fed.

The next feeding port is port 2. Different loss types are obtained at output ports of BM. At 2.4 GHz, the return loss S_{22} is about -24.7dB, which means that a good matching is achieved at the operating frequency. Insertion losses at the output ports of BM are about -6 dB. In addition, the average phase difference between output ports when port 2 is fed are about -134.12°. The simulation results in this case are summarized in Table 3.16.

Table 3.16: The insertion losses, return and isolation when port 2 is fed.

Input Port 2	Return Loss (dB)	Isolation Losses (dB)			Insertion Losses (dB)			
S_{ij}	2	1	3	4	5	6	7	8
	-24.7	**-28.6**	**-27.9**	**-28.0**	**-6.4**	**-6.4**	**-6.4**	**-6.2**

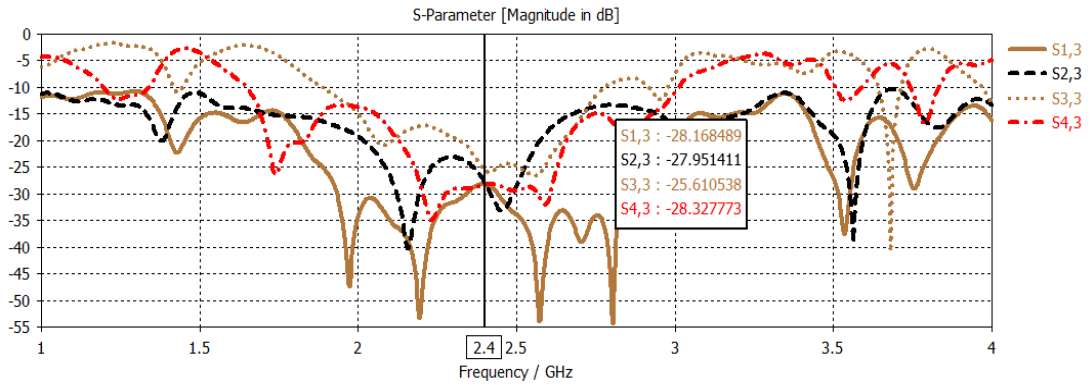

(g): Return and isolation losses when port 3 is fed.

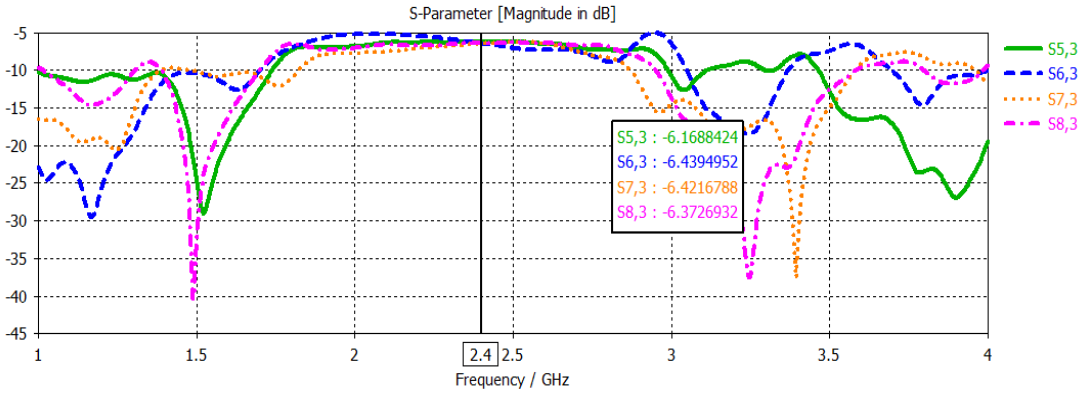

(h): Insertion losses when port 3 is fed.

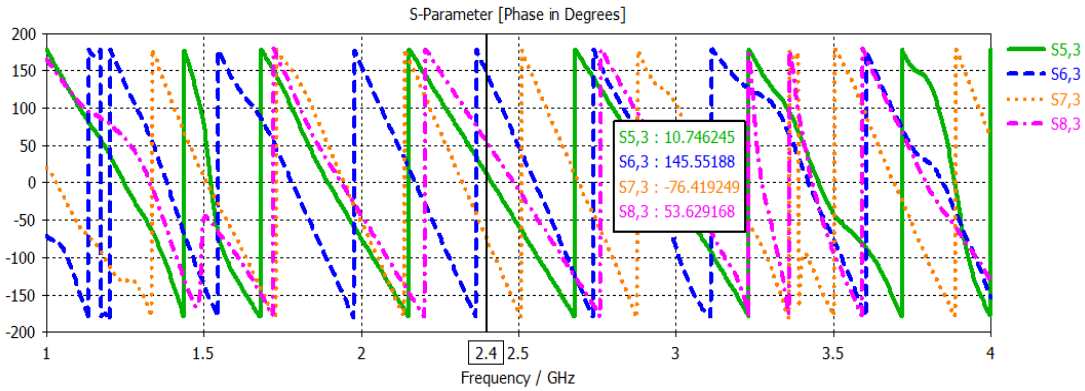

(i): Phase distribution of the output ports in case port 3 is fed.

As port 3 is excited, the simulation results are obtained at 2.4 GHz. The return loss S_{33} is around -25.6dB while the insertion losses are around -6dB as expected. The measured phase difference at the output of BM is about 134.29° that is closer to the theoretical calculations. Table 3.17 shows the above illustrations.

Table 3.17: Return, isolation and insertion losses when port 3 fed.

Input Port 3	Return Loss (dB)	Isolation Losses (dB)			Insertion Losses (dB)			
S_{ij}	3	1	2	4	5	6	7	8
	-25.6	**-28.1**	**-27.9**	**-28.3**	**-6.2**	**-6.4**	**-6.4**	**-6.3**

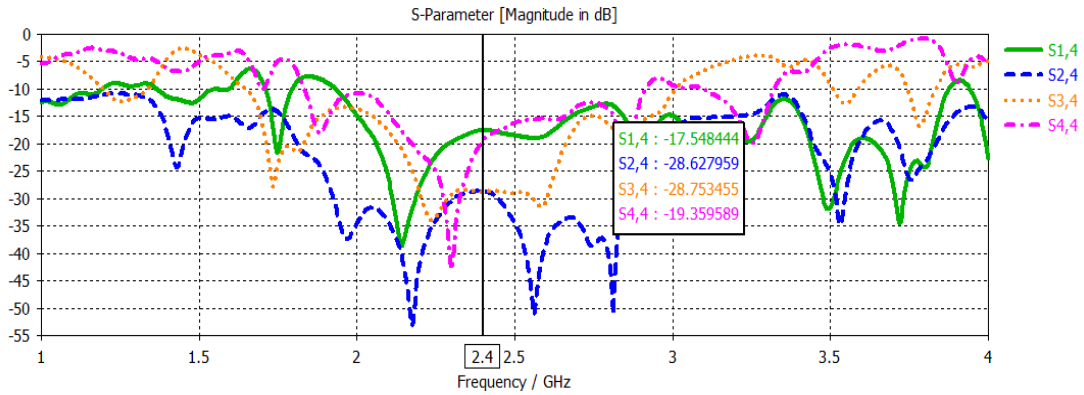

(j): Return and Isolation losses when port 4 is fed.

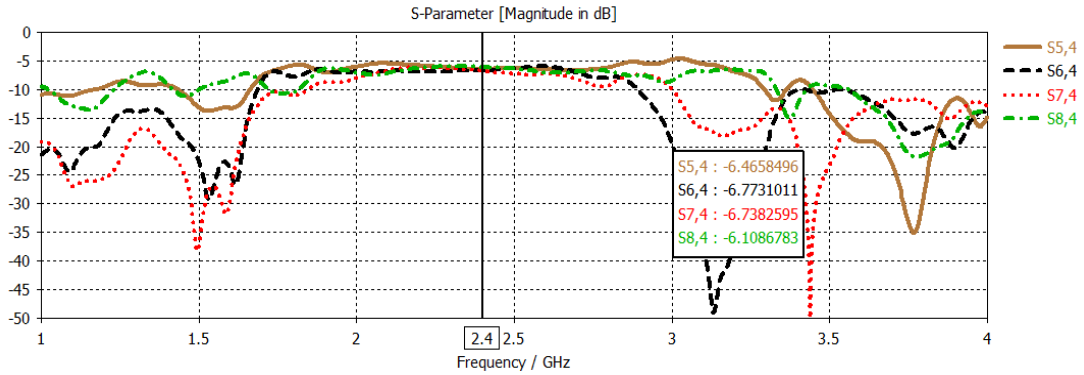

(k): Insertion losses when port 4 is fed.

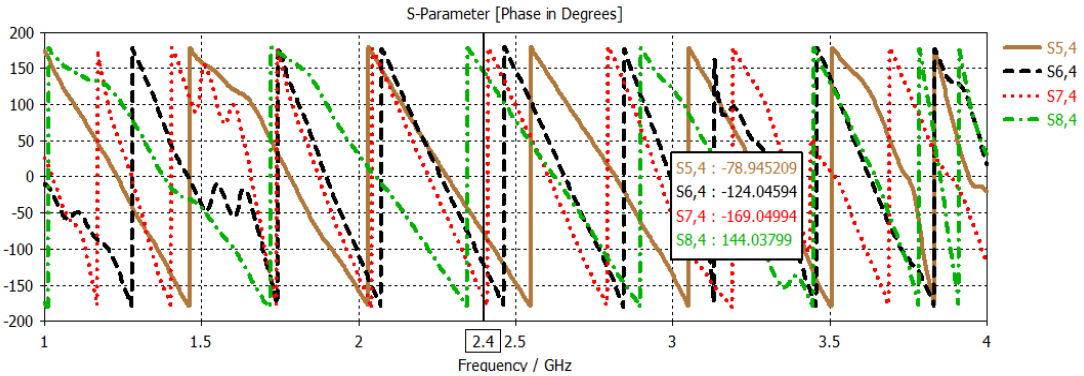

(l): Phase distribution of the output ports when port 4 is fed.

Figure 3.30: Return losses, isolation losses, insertion losses and phase shift at each output port when different input ports are fed.

Finally, the fourth port is fed. As shown from Figure 3.30.j, there is no mismatch occurred at the input port side since the return loss S_{44} is below -10dB. The insertion losses are close to -6dB while the phase difference between output ports when port 4

is fed is around -45.67° that assure the theoretical part of BM. Table 3.18 represents the above illustrations.

Table 3.18: Return, isolation and insertion losses when port 4 is fed.

Input Port 4	Return Loss (dB)	Isolation Losses (dB)			Insertion Losses (dB)			
S_{ij}	4	1	2	3	5	6	7	8
	-19.3	**-17.5**	**-28.6**	**-28.7**	**-6.5**	**-6.7**	**-6.7**	**-6.1**

From Figure 3.30, it is concluded that the return losses are better than -19dB when the signal is applied from different input ports. Moreover, the isolation among input ports and output ports are better than -20dB in general. In terms of insertion losses, all of them are around -6dB as expected. The average phase differences between output ports when the signal is applied from the input ports 1, 2, 3 and 4 were 45.7, -134.12°, 134.29° and -45.67°. Table 3.19 describes the phase difference between output ports when different input ports are fed.

Table 3.19: Phase shift between different ports of the BM.

Output Ports / Input Ports	Port 5	Port 6	Port 7	Port 8	φ average
Port 1	143.57°	-168.96°	-124.00°	-78.94°	45.7°
Port 2	53.14°	-76.32°	145°	10.78	-134.12°
Port 3	10.74°	145.55°	-76.41°	53.62°	134.29°
Port 4	-78.94°	-124.04°	-169.04°	144.03°	-45.67°

3.3.6 Antenna Design

In this section, a single element antenna is designed based on the shielding method and strip line technology. The idea in the shielding method is to implement the microwave

components of BM using proximity coupling technique. By using proximity coupling, a 13% fractional BW can be achieved as mentioned in Chapter 2, wherever the deployment of the antenna is different comparing it with the conventional patch. The antenna design is achieved by using an aperture at the top layer of the overall structure.

3.3.6.1 Antenna Design and Simulation Results Based on Shielding Method

Figure 3.31 shows a layout of a single element antenna for 2.4 GHz applications. The dimensions of the shielded antenna can be obtained by using microstrip line equations while the feed line dimensions can be calculated by using strip line equations. The antenna parameters and dimensions are introduced in Table 3.20.

Table 3.20: Shielded antenna structure dimension.

Parameter	Value
f_r	2.4 GHz
ε_r	2.2
h_1	0.8 mm
h_2	0.8 mm
Wf	1.2 mm
Li	12.75 mm
L	42.5 mm
W	49 mm
I	1.5 mm

The return loss and radiation pattern of the designed antenna are shown in Figures 3.32 and 3.33 respectively. In terms of the bandwidth, the proposed antenna has broader bandwidth compared with the conventional patch antenna due to the proximity coupling; however, such property for the shielding method in general depends on the type of the feeding network and the devices in the circuit. Circuits containing narrow band elements will have a narrow band overall response. The proposed structure has

lower side lobe levels than the conventional patch. Referring to Table 3.10, Table 3.21 shows a brief comparison between the microstrip antennas fed by microstrip line and the one fed by strip transmission line.

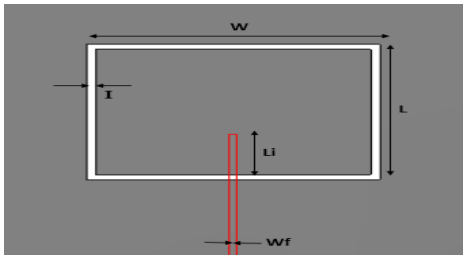

(a): Top view

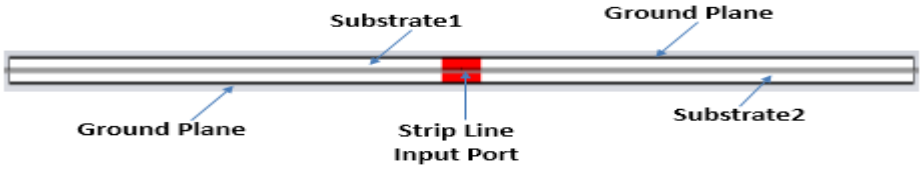

(b): Side view

Figure 3.31: Shielded antenna structure. (a): top view, (b): side view.

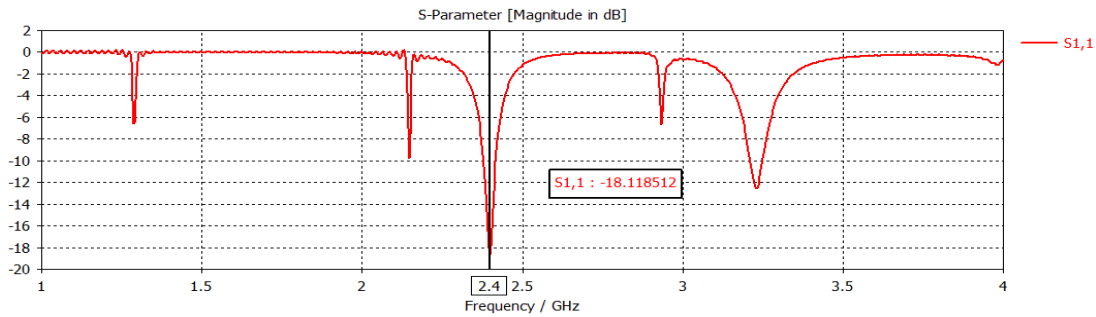

Figure 3.32: Shielded antenna return Loss.

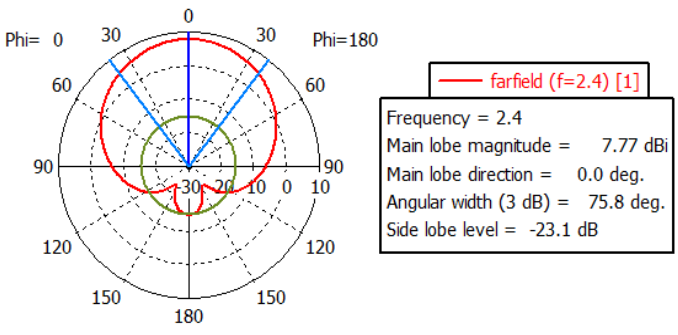

Figure 3.33: Shielded antenna radiation pattern.

Table 3.21: Comparison between conventional and proposed patch antenna.

Features	S_{11}	Directivity	SLL	HPBW	BW
Shielded	-18.1dB	7.77dBi	-23.1dB	75.8°	39.7 MHz
Conventional	-29.5dB	7.79dBi	-19.4dB	74.8°	36.6 MHz

3.3.7 Shielded Phased Antenna Array

In this section, shielded antenna array spaced by a half wavelength, which was designed in the previous section is combined directly to the designed 4×4 BM as shown in Figure 3.34.

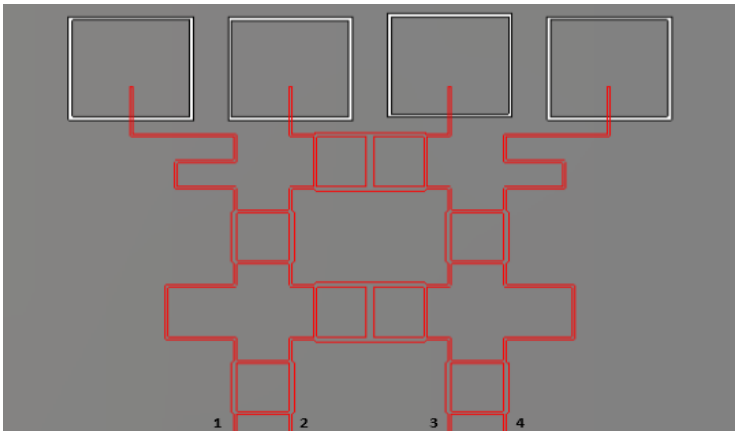

Figure 3.34: Phased antenna array based on modified BM and shielded array.

Different input ports will be applied to form a SBS as mentioned in Section 3.2.4 to obtain four orthogonal beams. Figures 3.35 and 3.36 show the radiation pattern characteristics in Cartesian coordinate system when ports 1and 4 are fed with signal while Figures 3.37 and 3.38 show the radiation pattern characteristics when ports 2 and 3are fed with signal.

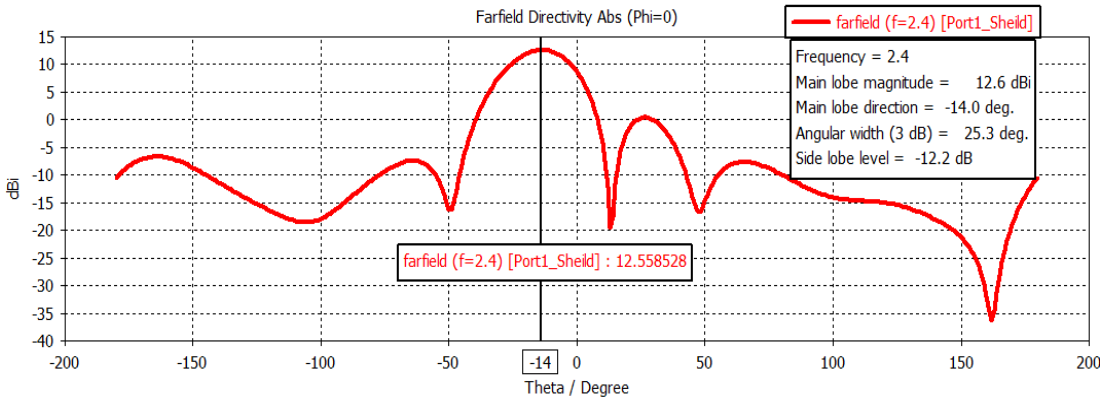

Figure 3.35: Radiation pattern of the modified structure when port 1 is fed.

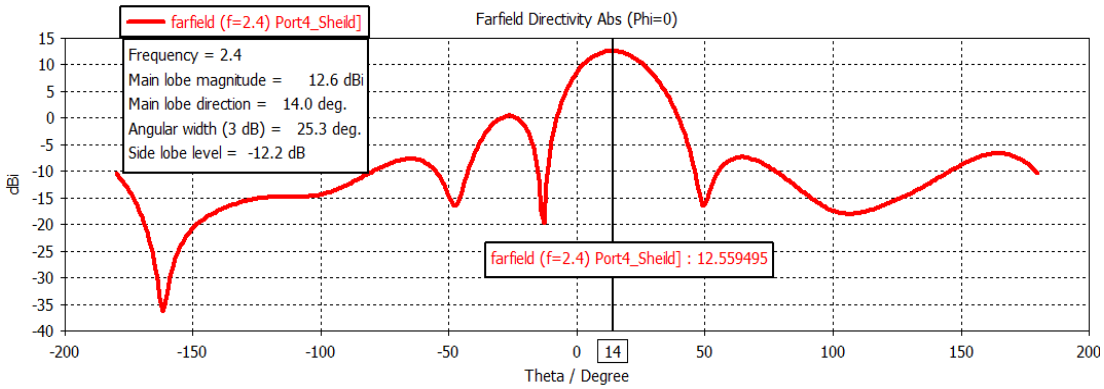

Figure 3.36: Radiation pattern of the modified structure when port 4 is fed.

In Figures 3.35 and 3.36, the main beam direction is switched to -14° and 14° when ports 1 and 4 are excited. Moreover, both radiation patterns have same directivity, but the sided lobes achieved have lower levels comparing with the conventional phased antenna array when the same ports are fed. The SLL's in both cases of feeding are -12.2dB. In terms of BW, both radiation patterns have narrow BW as shown in Figures 3.35 and 3.36 respectively.

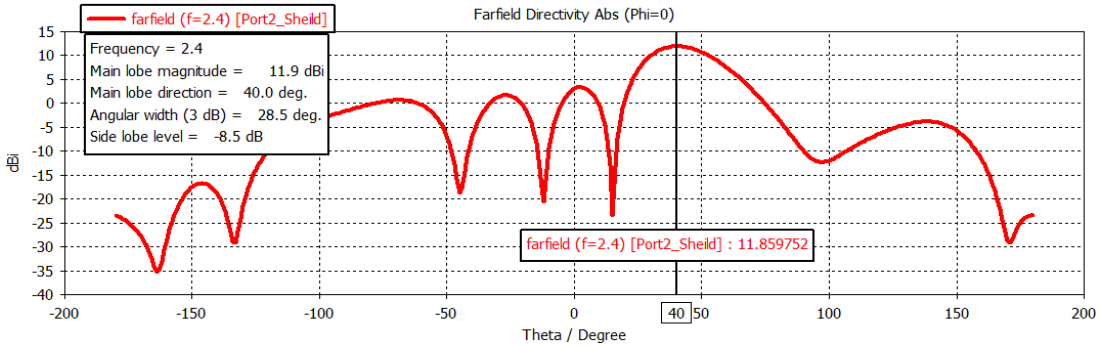

Figure 3.37: Radiation pattern of the modified structure when port 2 is fed.

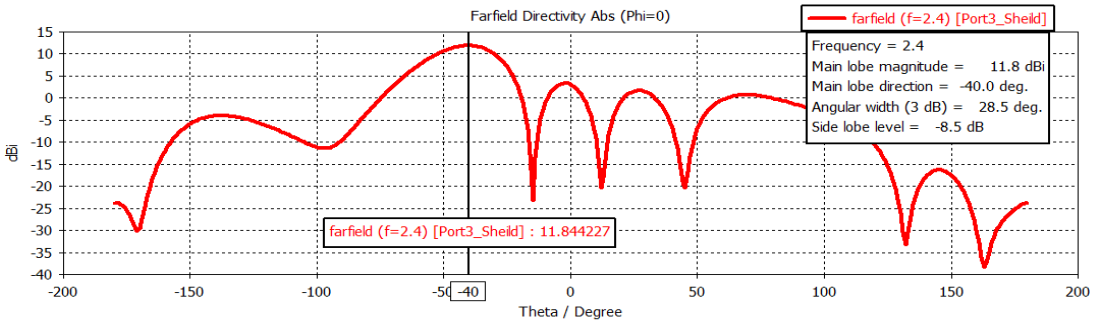

Figure 3.38: Radiation pattern of the modified structure when port 2 is fed.

When ports 2 and 3 are fed by signal, the main beam direction is switched to 40° and -40°. Both radiation patterns have the same directivity with acceptable levels of side lobe levels. -8.5dB SLL's are achieved in both cases of feeding with narrow BW as shown in Figures 3.34 and 3.35.

Finally, the four radiation patterns are plotted in Cartesian coordinate system when different input ports were applied as shown in Figure 3.39. The features of this system can be summarized in Table 3.22.

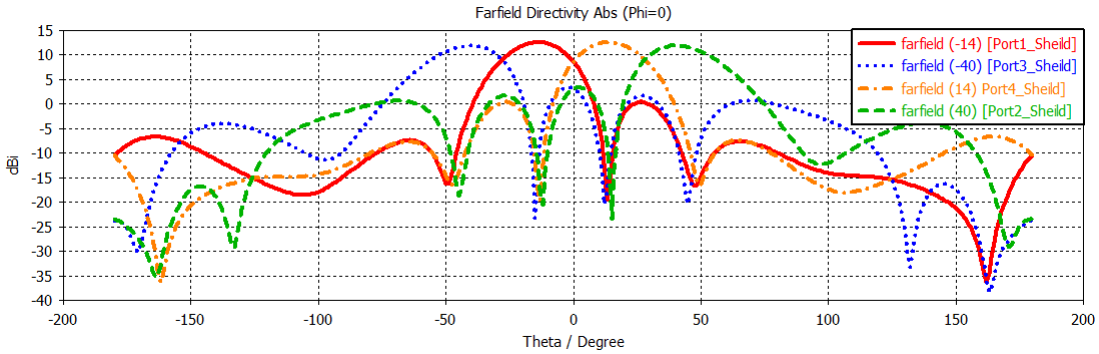

Figure 3.39: Four radiation patterns when different input ports were applied in Cartesian coordinate system.

Table 3.22: Phased antenna array based on modified BM.

Features	**Phased Antenna Array using B.M**
Center Frequency	2.4
Physical Size	18.5cm×23.6cm
Antenna Directivity: $\boldsymbol{\varphi = \pm 45}$ $\boldsymbol{\varphi = \pm 135}$	 12.6 dBi 11.9 dBi
Spatial Scan Coverage	107.6°
Maximum scan angle: $\boldsymbol{\varphi = \pm 45}$ $\boldsymbol{\varphi = \pm 135}$	 $\pm$14 $\pm$40
S.L.L: $\boldsymbol{\varphi = \pm 45}$ $\boldsymbol{\varphi = \pm 135}$	 -12.2 dB -8.5 dB

3.3.8 Comparison between the Conventional and Shielded Designs

Due to the shielding method, the radiation loss of feeding network is reduced by the strip line technology. As expected, the radiation loss is reduced comparing with the conventional feeding network based on microstrip technology, also, the side lobe and minor lobe levels are reduced.

A comparison between conventional and modified phased antenna array based on strip line technology is done focused on SLL, directivity, physical size and spatial scan coverage for both designs when different input ports are applied.

Figures 3.40, 3.41, 3.42 and 3.43 show the radiation patterns when ports 1, 2, 3 and 4 were applied for both structures.

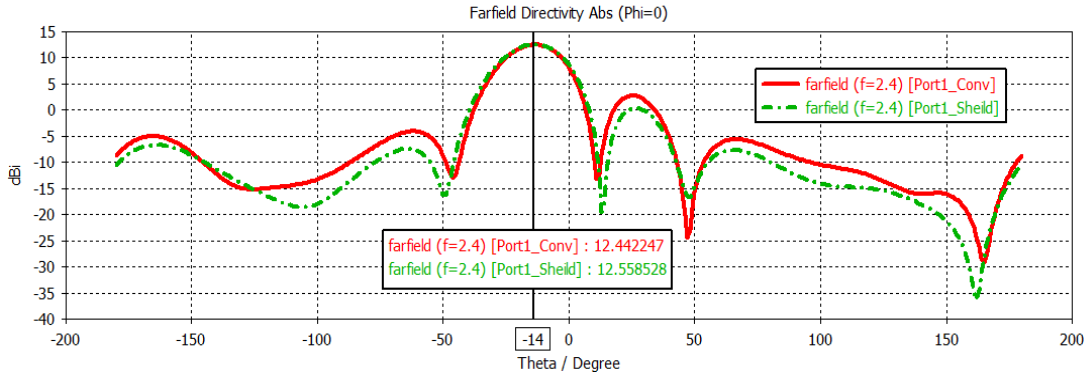

Figure 3.40: Radiation patterns in Cartesian coordinate system for shielded and conventional phased antenna array when port 1 was fed.

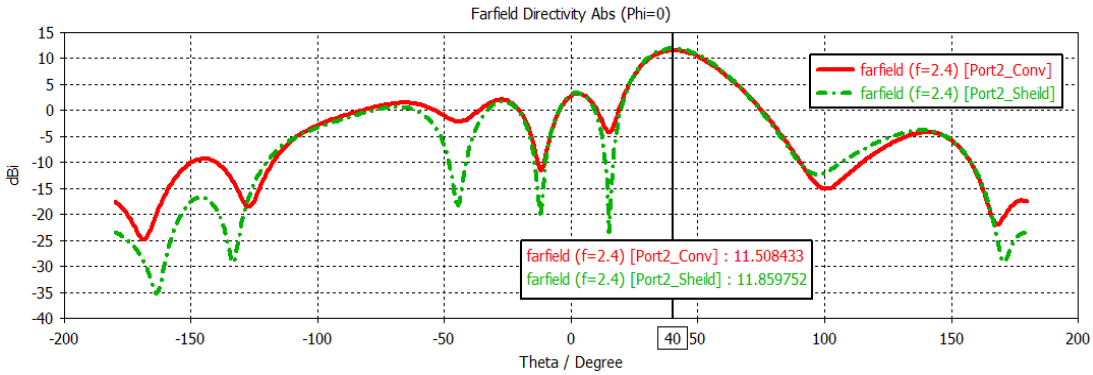

Figure 3.41: Radiation patterns in Cartesian coordinate system for shielded and conventional phased antenna array when port 2 was fed.

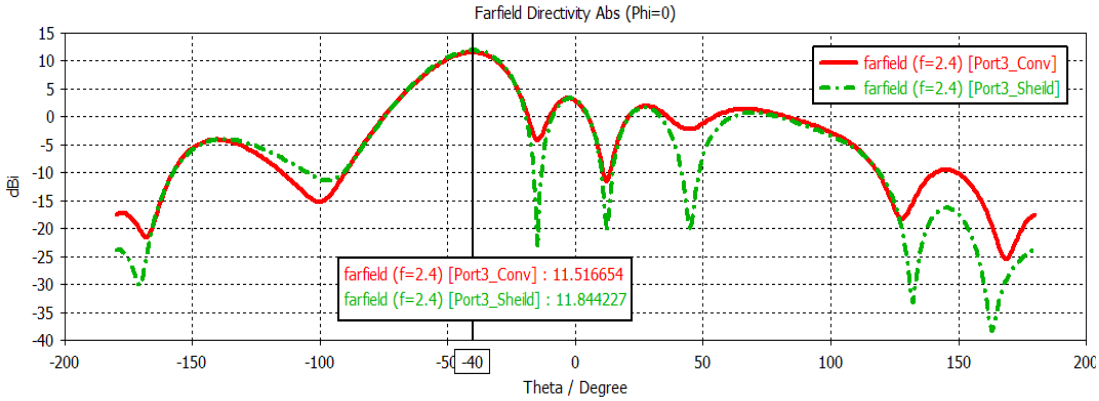

Figure 3.42: Radiation patterns in Cartesian coordinate system for shielded and conventional phased antenna array when port 3 was fed.

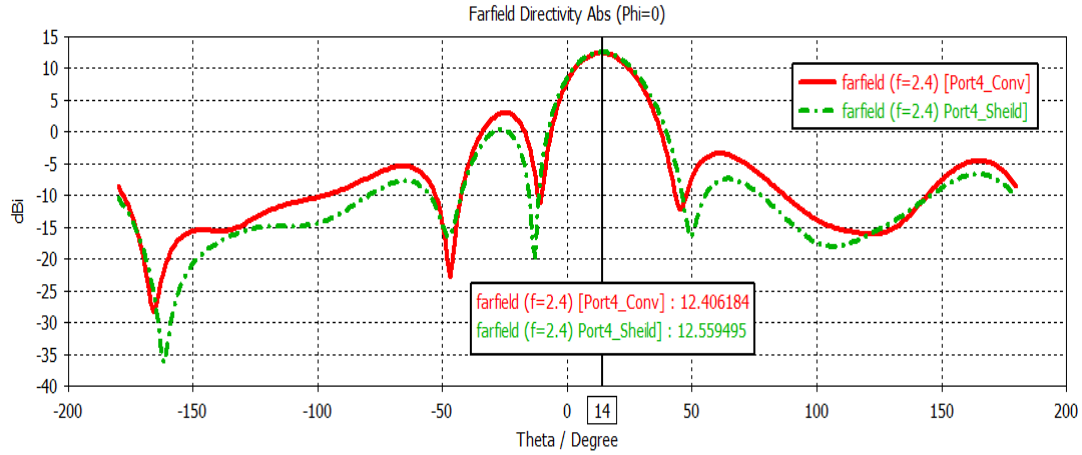

Figure 3.43: Radiation patterns in Cartesian coordinate system for shielded and conventional phased antenna array when port 4 was fed.

From Figures 3.40, 3.41, 3.42 and 3.43, it is clear that the shielded structure has lower level of side lobes than the conventional structure, which in turn could enhance the SBS performance. Moreover, an increment on directivity is achieved for the shielded system, and hence, the antenna gain will be increased spontaneously.

The shielded system has deeper nulls comparing with the conventional one, which in turn can enhance the shape of main lobe at different directions when different input ports are applied, and hence, the detection of the target will be more accurate than using the conventional design.

The physical size of the shielded design was smaller than the conventional design obtained by using the strip lines instead of microstrip lines. Table 3.23 shows a summary of the obtained results and improvements achieved in terms of the radiation parameters when shielded phased antenna array based on strip line BM is used.

Table 3.23: Summary of results.

Features		**Design**	
		Conventional Design	**Modified Design**
ε_r		2.2	2.2
h		1.6 mm	1.6 mm
f_r		2.4 GHz	2.4 GHz
Physical Size		(27×23) cm	(18.5×23.6) cm
Directivity	$\boldsymbol{\varphi = \pm 45^{\circ}}$ $\boldsymbol{\varphi = \pm 135^{\circ}}$	12.4 dBi 11.5 dBi	12.6 dBi 11.9 dBi
S.L.L	$\boldsymbol{\varphi = \pm 45^{\circ}}$ $\boldsymbol{\varphi = \pm 135^{\circ}}$	-9.4 dB -8.2 dB	-12.2 dB -8.5 dB
Scan Angle	$\boldsymbol{\varphi = \pm 45^{\circ}}$ $\boldsymbol{\varphi = \pm 135^{\circ}}$	$\pm 14^{\circ}$ $\pm 40^{\circ}$	$\pm 14^{\circ}$ $\pm 40^{\circ}$
Scan Coverage		106.8°	107.6°

Chapter 4

CONCLUSION

In this work, a method is used to shield the radiation pattern of BM to reduce the radiation loss of the microstrip line technology feed network. The shielded phased antenna structure design based on the proximity coupling design has better performance compared with the conventional one based on microstrip technology in terms of SLL and directivity. The SLL is dropped by 2.8dB when ports 1 and 4 are excited by a sinusoidal signal and 0.3dB when ports 2 and 3 are the excitation ports. This enhancement is useful to prevent grating lobes to appear in the radiation pattern. The scan angle for both designs have the same direction when different input ports are applied. Moreover, deeper nulls are obtained when shielding method is applied on phased antenna array structure.

The physical size of the structure is also reduced; the overall size structure of shielded design is smaller than the conventional structure based on microstrip line technology. (18.5×23.6) cm^2 structure size is obtained when shielded method is used while (27×23) cm^2 structure size is obtained when microstrip line technology is used to design the phased antenna array. 184 cm^2 size reduction is achieved, and hence, it will be easy to implement it in any 2.4 GHz communication system.

REFERENCES

[1] C. A. Balanis and I. Panayiotis I, "Introduction to smart antennas," vol. 2, no. 1, pp. 1-175, 2007.

[2] C. A. Balanis, Antenna theory: analysis and design, John Wiley & Sons, 2016.

[3] W. Bernard, P. Mantey and L. a. Griffiths, "Adaptive antenna system," *Proceedings of the IEEE,* vol. 55, no. 12, pp. 2143-2159, 1967.

[4] W. Gabriel, "Preface-Special issue on adaptive antennas," *IEEE Transactions on Antennas and Propagation,* vol. 24, no. 5, pp. 573-574, 1976.

[5] R. Schmidt, "Multiple emitter location and signal parameter estimation," *IEEE transactions on antennas and propagation,* vol. 34, no. 3, pp. 276-280, 1986.

[6] Alam, Muhammad Mahfuzul, "Microstrip antenna array with four port butler matrix for switched beam base station application," in *Computers and Information Technology ICCIT'09. 12th International Conference on*, 2009.

[7] F. Shaikh and S. B. Akhade, "Smart Antenna System using 4x4 Butler Matrix switched beam network for 2.4 GHz ISM band," vol. 4, no. 3, pp. 278-282, March 2015.

[8] H. Mirmohammad Sadeghi, M. Moradianpour, M. a. A. G. Hedayati and P. Moslemi, "Design and Implementation of a Compact Practical Passive Beam-Forming Matrix for 3D S-Band Radar," *Progress In Electromagnetics Research B*, vol. 61, pp. 225-239, 2014.

[9] T. N. Kaifas and J. N. Sahalos, "On the design of a single-layer wideband Butler matrix for switched-beam UMTS system applications [Wireless Corner]," *IEEE Antennas and Propagation Magazine*, vol. 48, no. 6, pp. 193-204, 2006.

[10] S. Z. Ibrahim and M. K. A. Rahim, "Switched beam antenna using omnidirectional antenna array," in *Applied Electromagnetics, 2007. APACE 2007. Asia-Pacific Conference on*, 2007.

[11] j. Butler and R. Lowe, "Beam-forming matrix simplifies design of electronically scanned antennas," *Electronic Design 9*, pp. 170-173, 1961.

[12] K. Debbarma, T. Moyra and D. Yadav, "Size Reduction of 4×4 Butler Matrix Using Defected Microstrip Structure," in *Emerging Trends in Computing and Communication*, 2014.

[13] H. Nachouane, A. Najid, A. Tribak and F. Riouch, "Broadband 4×4 Butler matrix using wideband 90° hybrid couplers and crossovers for beamforming networks," in *Multimedia Computing and Systems (ICMCS), International Conference on*, 2014.

[14] Y. Zhai, X. Fang, K. Ding and F. He, "Miniaturization Design for 8×8 Butler Matrix Based on Back-to-Back Bilayer Microstrip," vol. 8, 2014

[15] B. Sahu, "Design and Implementation of 4x4 Butler Matrix".

[16] W.-R. Li, C.-Y. Chu, K.-H. Lin and S.-F. Chang, "Switched-beam antenna based on modified Butler matrix with low sidelobe level," *Electronics Letters*, vol. 40, no. 5, pp. 290-292, 2004.

[17] F. E. Fakoukakis, G. A. Kyriacou and J. N. Sahalos, "On the design of Butler-like type matrices for low SLL multibeam antennas," in *Antennas and Propagation (EUCAP), 2012 6th European Conference on*, 2012.

[18] T. A. a. L. T. E. Denidni, "Wide band four-port butler matrix for switched multibeam antenna arrays," in *Personal, Indoor and Mobile Radio Communications, 2003. PIMRC 2003. 14th IEEE Proceedings on*, 2003.

[19] R. J. Collier and A. D. Skinner, Microwave measurements, vol. 12, IET, 2007.

[20] R. E. Collin, Foundations for microwave engineering, John Wiley & Sons, 2007.

[21] Y. Huang and K. Boyle, Antennas: from theory to practice, John Wiley & Sons, 2008.

[22] M. Ali, S. Muhamud, N. A. Rahman and N. Ya'acob, "A microstrip patch antenna with aperture coupler technique at 5.8 GHz," in *System Engineering and Technology (ICSET), IEEE International Conference on*, 2011.

[23] S. S. Chakravarthy, N. Sarveshwaran, S. Sriharini and M. Shanmugapriya, "Comparative study on different feeding techniques of rectangular patch antenna," in *Wireless and Optical Communications Networks (WOCN), Thirteenth International Conference on*, 2016.

[24] I. R. Sastry and K. J. Sankar, "Proximity Coupled Rectangular Microstrip Antenna with X-slot for WLAN Application," *Global Journal of Research and Engineering-GJRE-F,* vol. 14, no. 1, 2014.

[25] K. Carver and J. Mink, "Microstrip antenna technology," *IEEE transactions on antennas and propagation,* vol. 29, no. 1, pp. 2-24, 1981.